The background of the image is a dark blue to black gradient, representing the void of space. Scattered throughout are numerous small, glowing stars of varying sizes and colors. In the upper right quadrant, there is a prominent, large nebula. It has a bright, yellowish-orange center that transitions into a greenish-blue hue towards the edges. The nebula appears to be a dense cluster of gas and dust, with some darker, shadowed regions where the gas density is higher.

KRITIKA SUMMER PROJECTS 2020

# Exoplanets

Ananya Biswas, Arnav Das, Joy, Nitish, Pragya,  
Praneet, Devansh Jain, Vaishnav Rao, and Sagar



KRITTIKA SUMMER PROJECTS 2020

# Exoplanets

Ananya Biswas<sup>4</sup>, Arnav Das<sup>3</sup>, Joy<sup>2</sup>, Nitish<sup>2</sup>, Pragya<sup>2</sup>, Praneet<sup>2</sup>, Devansh Jain<sup>1,2</sup>, Vaishnav Rao<sup>1,2</sup>, and Sagar<sup>1,2</sup>

<sup>1</sup>Krittika - The Astronomy Club of IIT Bombay, Powai, Mumbai - 400076, India

<sup>2</sup>Indian Institute of Technology Bombay, Mumbai - 400076, India

<sup>3</sup>Hiranandani Foundation School, Powai, Mumbai - 400076, India

<sup>4</sup>Maulana Azad College, Kolkata - 700013, India

Copyright © 2020 Krittika IITB

PUBLISHED BY KRITTIKA: THE ASTRONOMY CLUB OF IIT BOMBAY

[GITHUB.COM/KRITTIKAIITB](https://github.com/KRITTIKAIITB)

First Release, August 2020

# Abstract

Search for Exoplanets is a hot topic of research in the field of Astronomy.

This is the report of the Exoplanets Project done as part of the Krittika Summer Projects, conducted by Krittika, The Astronomy Club of IIT Bombay and mentored by Sagar Kumar Gupta. It describes the different Methods used to detect Exoplanets, followed by modelling of Light Curve of Multiple Exoplanet systems and finally Data Analysis using Markov Chain Monte Carlo methods.

To date (August 2020), 4302 exoplanets have been confirmed, belonging to 3177 planetary systems of which 703 are multiple planet systems. More than 888 have been observed through radial velocity measurements, at least 140 by Direct Imaging, 125 by Microlensing (Gravitational Lensing), 43 by Pulsar Timings. The transits of almost 4000 of them have been observed. (<http://exoplanet.eu/>, 2020)

The first Chapter is a short introduction to the field of discovery of Exoplanets.

The second Chapter describes five most commonly used methods of detection of Exoplanets - Transit Light Curve, Radial Velocity, Gravitational Lensing, Direct Imaging and Pulsar Imaging. The first two methods are discussed in detail resulting in a proper model incorporating factors like Eccentricity of orbit and Limb Darkening of star. Gravitational Lensing (Microlensing) uses the General Theory of Relativity and is described in detail with derivations of a simple model. Principles of Direct Imaging and Pulsar Imaging are briefly described towards the end of the chapter.

The third Chapter is about modelling the Light Curve for a multi-planetary system. The chapter includes derivation of the model and its resultant plots, this model is applied to Trappist-1 system (planetary system with seven discovered earth sized planet). Chapter ends with drawing inferences about the properties of the system through its light curve.

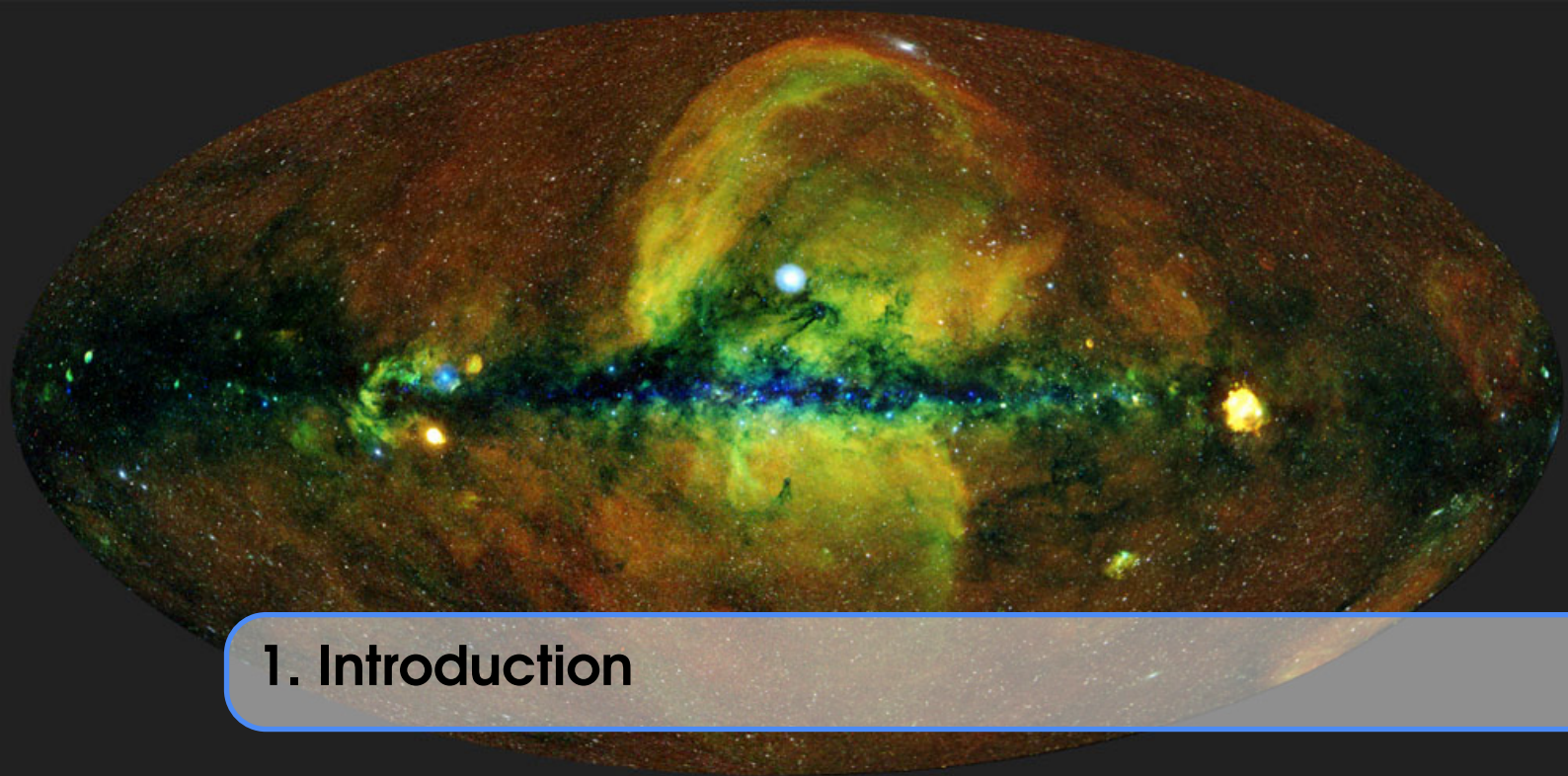
The fourth Chapter describes how we fitted our Transit Light Curve model to real data and inferred the parameters of the exoplanet system using inferential statistics. The chapter includes a brief overview of the model used, an introduction to Bayesian statistics, a description of Markov Chain Monte Carlo methods, how the Metropolis-Hastings Algorithm was implemented for our particular model, the various challenges faced during implementation, and a brief discussion on improving the process of parameter inference.



# Contents

<b>1</b>	<b>Introduction</b>	<b>5</b>
<b>2</b>	<b>Methods of Exoplanet Detection</b>	<b>6</b>
<b>2.1</b>	<b>Transit Light Curve</b>	<b>6</b>
2.1.1	Introduction	6
2.1.2	Background	6
2.1.3	Orbital Parameters	7
2.1.4	Rotation and Euler angles	9
2.1.5	Simulation	10
2.1.6	Limb Darkening	10
2.1.7	Limb darkening effect in transiting exoplanet	10
2.1.8	Thermal emission and reflected light from exoplanets	13
2.1.9	Incorporation of limb darkening and other phenomena in the simulation	13
<b>2.2</b>	<b>Radial Velocity</b>	<b>16</b>
2.2.1	Introduction	16
2.2.2	Doppler effect	16
2.2.3	Radial Velocity method	17
2.2.4	Simulation and Plots	20
2.2.5	Radial Velocity Method for an Elliptical Orbit	21
<b>2.3</b>	<b>Gravitational Lensing</b>	<b>24</b>
2.3.1	Introduction	24
2.3.2	Theory	25
2.3.3	Simulation	29
<b>2.4</b>	<b>Direct Imaging</b>	<b>31</b>
<b>2.5</b>	<b>Pulsar Timing</b>	<b>32</b>
<b>2.6</b>	<b>Conclusion</b>	<b>33</b>

<b>3</b>	<b>Multiple Exoplanets .....</b>	<b>35</b>
<b>3.1</b>	<b>New Approach to Transit Light Curve</b>	<b>35</b>
3.1.1	Finding the True Anomaly .....	36
3.1.2	Finding position of the Planet .....	36
3.1.3	Imaging Method to calculate luminosity .....	37
<b>3.2</b>	<b>Plots</b>	<b>38</b>
3.2.1	True Anomaly Vs Time .....	38
3.2.2	Orbit Coordinates .....	39
3.2.3	Imaging Method .....	40
3.2.4	Transit Light Curve for Multiple Exoplanets system .....	41
<b>3.3</b>	<b>Case Study : TRAPPIST-1 System</b>	<b>42</b>
<b>3.4</b>	<b>Inferences</b>	<b>43</b>
<b>4</b>	<b>Data Analysis .....</b>	<b>44</b>
<b>4.1</b>	<b>Introduction</b>	<b>44</b>
<b>4.2</b>	<b>Bayesian Statistics</b>	<b>45</b>
4.2.1	Bayes' formula .....	46
4.2.2	Why the Bayesian approach preferred? .....	46
<b>4.3</b>	<b>Markov Chain Monte Carlo</b>	<b>46</b>
4.3.1	The Metropolis-Hastings Algorithm .....	47
<b>4.4</b>	<b>Implementation</b>	<b>48</b>
<b>4.5</b>	<b>Plots</b>	<b>48</b>
<b>4.6</b>	<b>Inference</b>	<b>49</b>
<b>4.7</b>	<b>Challenges</b>	<b>50</b>
<b>4.8</b>	<b>Discussion</b>	<b>51</b>
	<b>References .....</b>	<b>52</b>



## 1. Introduction

Since time immemorial, whenever mankind has looked upon the night sky and has seen the beauty of the universe, he has always wondered - Are we alone?

This quest, to answer this question, has been extant for millennia. We tried finding planets like our own Earth in our own system, and this can be seen in the Roman and Greek names of the planets - Mercury, Venus, Mars, Jupiter, Saturn, Uranus, etc.

And thus the next logical leap in questioning of our existence came - Are there similar planets orbiting stars other than our Sun?

This question can be best answered by Giordano Bruno, an Italian philosopher, mathematician and cosmological theorist, and an early supporter of heliocentrism, who stated that -

*This space we declare to be infinite...  
In it are an infinity of worlds of the same kind as our own.*

And thus, after hypothesizing the existence of other planets outside the Solar System, around other stars in the night sky, for centuries, the first confirmed discovery came in 1992, by [Wolszczan & Frail \(1992\)](#). In 1995, Michel Mayor and Didier Queloz discovered 51 Pegasi b, the first extrasolar planet orbiting a sun-like star, 51 Pegasi ([Mayor & Queloz \(1995\)](#)) and this earned them the Nobel Prize in Physics in 2019.

Since then, the past 3 decades have been extremely busy, leading to confirmed discovery of more than 4000 exoplanets. These discoveries are made through several proved scientific methods; a few of these have been explained further.

## 2. Methods of Exoplanet Detection

### 2.1 Transit Light Curve

#### 2.1.1 Introduction

When a planet passes between its host star and an observer, it blocks some of the light received by the observer. Thus, a distinct dip is seen in the light curve of the host star. This dip can be used to find the dimensions of the planet, its orbital parameters, etc. as well as confirm the existence of the exoplanet.

#### 2.1.2 Background

Consider 2 circles, with radius  $r_1$  and  $r_2$  and the distance between the centres as  $d$ . Without loss of generality, let  $r_2 \leq r_1$ . Then the area of overlap between these circles

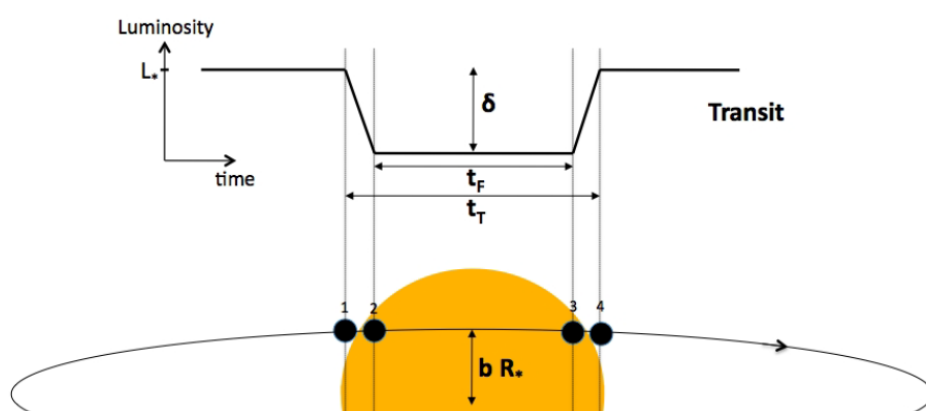


Figure 2.1: The schematic of a planet transiting its host star with the corresponding variation in brightness during the transit. (Alapini Odunlade (2010))

$(A_{\text{intersection}})$  can be calculated.

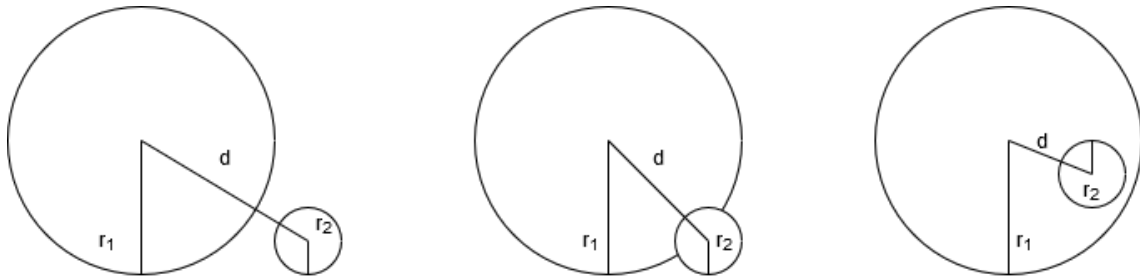


Figure 2.2: Three cases of intersecting circles

1. If  $d \geq r_1 + r_2$ , the circles do not overlap and  $A_{\text{intersection}} = 0$
2. If  $d \leq r_1 - 2r_2$ ,  $A_{\text{intersection}} = \pi r_2^2$  as the smaller circle lies entirely within the bigger circle
3. Else, if  $d_1 = \frac{r_1^2 - r_2^2 + d^2}{2d}$  and  $d_2 = d - d_1 = \frac{r_2^2 - r_1^2 + d^2}{2d}$ , then

$$A_{\text{intersection}} = r_1^2 \cos^{-1} \left( \frac{d_1}{r_1} \right) - d_1 \sqrt{r_1^2 - d_1^2} + r_2^2 \cos^{-1} \left( \frac{d_2}{r_2} \right) - d_2 \sqrt{r_2^2 - d_2^2} \quad (2.1)$$

This equation would be used when considering the amount of light of the host star blocked by the planet, for the simulation of the transit method.

### 2.1.3 Orbital Parameters

Kepler mentioned in his laws of planet motion that a planet orbits a host star in an elliptical orbit, with the host star at one of the foci of the ellipse. To define the elliptical orbit of a planet around a star, you need 6 independent parameters. These parameters define a unique orbit. This is because there are 6 degrees of freedom - 3 spatial dimensions ( $x, y, z$  components if a Cartesian co-ordinate system is used) and the velocity along each of these directions. However, Keplerian elements are generally used, as they can be easy to use for any orbit as seen in the night sky.

The major parameters of an orbit are -

1. Semi-major axis ( $a$ ) - This refers to the maximum distance any point on the ellipse is from the centre of the ellipse. Thus, just as the radius is a parameter to indicate the size of a circle, semi-major axis is a parameter for the size of the ellipse. This is a Keplerian element.
2. Eccentricity ( $e$ ) - This indicates the flatness/elongation of the ellipse compared to a circle. Eccentricity lies between 0 and 1. An eccentricity of 0 indicates a circle. This is a Keplerian element.
3. Eccentric anomaly ( $E$ ) - The basic equation of an ellipse is written as

$$\frac{x^2}{a^2} + \frac{y^2}{b^2} = 1 \quad (2.2)$$

$$(b = a\sqrt{1 - e^2}) \quad (2.3)$$

Thus, a parametric equation given below satisfies the equation of the ellipse. Here,  $E$  can lie anywhere between 0 and  $2\pi$ . Notice the similarity with the

parametric coordinates of a point on the auxiliary circle.

$$(x, y) = (a \cos(E), b \sin(E)) \quad (2.4)$$

Mean anomaly is also a parameter of significant importance. It is given by -

$$M = 2\pi \frac{t}{P} = E - e \sin(E) = \frac{2A}{ab} \quad (2.5)$$

$M$  = Mean anomaly

$P$  = period of the orbit

$t$  = time

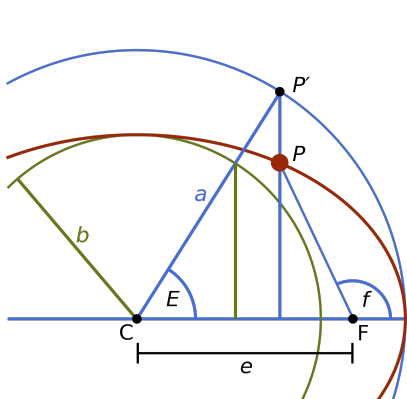
$A$  = Area covered by radial vector (calculated with host star as origin)

These equations are indicative of the second Kepler's law of planetary motion

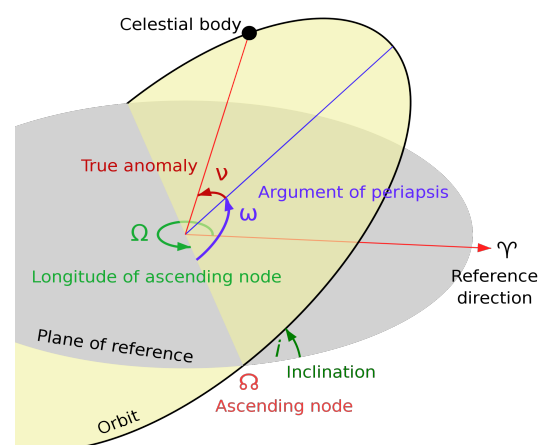
- *A line segment joining a planet and the Sun sweeps out equal areas during equal intervals of time.*

In the above equations, the area covered and time elapsed can easily be observed to be linear. Therefore, equal intervals of time leads to equal area covered.

4. Inclination ( $i$ ) - The point at which the orbit of the planet passes through the reference plane (a patch on the celestial sphere or the night sky as seen from the earth) is called the ascending node. The tilt of the elliptical orbit with respect to the reference plane, as measured at the ascending node, is called the inclination. The value lies between  $0^\circ$  to  $90^\circ$  (both inclusive).  $0^\circ$  inclination indicates an orbit lying in the reference plane. This is a Keplerian element.
5. Longitude of the ascending node ( $\Omega$ ) - The angle which the ascending node makes with the reference direction of the reference plane is called the longitude of the ascending node. Its value lies  $\in [0^\circ, 360^\circ]$ . It is used to orient the orbit through rotation about a vector perpendicular to the reference plane. This is a Keplerian element.



(a) A figure showing eccentric anomaly.



(b) A figure showing the important Keplerian elements.

6. Argument of periapsis ( $\omega$ ) - It represents a rotation about the vector perpendicular to the orbital plane. Its value lies  $\in [0^\circ, 360^\circ]$ . It can be measured as the angle between the periapsis (the point of the orbit where the distance

between the exoplanet and the host star is minimum) and the ascending node. This is a Keplerian element.

Thus, the steps we follow to create an ellipse in 3D is -

1. Use  $a$  and  $e$  to calculate  $b$  (semi-minor axis) using 2.3.
2. Thus, individual points on the ellipse are found by using 2.4, where  $E$  varies from 0 to  $2\pi$ .
3. These points still lie on the reference plane, which in this case, is the  $xy$ -plane. Using the remaining three parameters -  $i$ ,  $\Omega$ ,  $\omega$ , we can rotate these points in any orientation necessary. This is performed by Euler Angles.

#### 2.1.4 Rotation and Euler angles

Consider a  $xy$ -plane, with the  $z$ -axis pointing out of the plane. For a counterclockwise rotation of the coordinate system around the  $z$ -axis by angle  $\theta$ , the new coordinates  $(xn, yn)$  of points  $(x, y)$  in the original plane are given by -

$$(xn, yn) = (x \cos(\theta) + y \sin(\theta), -x \sin(\theta) + y \cos(\theta)) \quad (2.6)$$

This can be represented as -

$$\begin{bmatrix} xn \\ yn \end{bmatrix} = \begin{bmatrix} \cos(\theta) & \sin(\theta) \\ -\sin(\theta) & \cos(\theta) \end{bmatrix} \begin{bmatrix} x \\ y \end{bmatrix} \quad (2.7)$$

In 3-D, this can be written as -

$$\begin{bmatrix} xn \\ yn \\ zn \end{bmatrix} = \begin{bmatrix} \cos(\theta) & \sin(\theta) & 0 \\ -\sin(\theta) & \cos(\theta) & 0 \\ 0 & 0 & 1 \end{bmatrix} \begin{bmatrix} x \\ y \\ z \end{bmatrix} \quad (2.8)$$

Thus, the matrix  $\begin{bmatrix} \cos(\theta) & \sin(\theta) & 0 \\ -\sin(\theta) & \cos(\theta) & 0 \\ 0 & 0 & 1 \end{bmatrix}$  is used for rotation about  $z$ -axis by angle  $\theta$ .

This matrix can be represented as  $R_z(\theta)$ . Similarly,

$$R_y(\theta) = \begin{bmatrix} \cos(\theta) & 0 & \sin(\theta) \\ 0 & 1 & 0 \\ -\sin(\theta) & 0 & \cos(\theta) \end{bmatrix} \text{ and } R_x(\theta) = \begin{bmatrix} 1 & 0 & 0 \\ 0 & \cos(\theta) & \sin(\theta) \\ 0 & -\sin(\theta) & \cos(\theta) \end{bmatrix}$$

Any reference  $xyz$ -coordinate system can be converted into another orientation, by rotation around the axes. Euler angles are three angles to describe the orientation of a rigid body with respect to a fixed coordinate system. This system involves  $xyz$ -reference system and  $XZY$ -target system and three rotations. We need to orient the reference system so that it becomes the target system using these 3 rotations. The successive orientations steps are as follows -

1. After the first rotation around any one of the principle vectors of the  $xyz$ -system,  $xyz$ -system converts to  $x^1y^1z^1$ -system.
2. After the second rotation around any one of the principle vectors of the  $x^1y^1z^1$ -system,  $x^1y^1z^1$ -system converts to  $x^2y^2z^2$ -system.
3. After the third rotation around any one of the principle vectors of the  $x^2y^2z^2$ -system,  $x^2y^2z^2$ -system converts to  $XZY$ -system.

The norm used is the  $z-x-z$  system. This means that the first rotation is carried around the  $z$ -axis (using  $R_z$ ), the second rotation is carried around the  $x^1$  axis (using  $R_{x^1}$ ), and the third rotation is carried around the  $z^2$  axis (using  $R_{z^2}$ ).

### 2.1.5 Simulation

Using the above procedure, the orbit of a planet can easily be simulated.

1. Assign the radius of the star and the planet, and the parameters  $a, e, i, \Omega, \omega$  necessary to simulate the orbit.
2.  $E$  is varied from 0 to  $\pi$ . We use  $\pi$  and not  $2\pi$  as we consider only the situation when the planet obscures the sun, and not vice versa. Thus, only half of the orbit needs to be considered. At each value of  $E$ ,  $M$  and  $t$  are calculated using equation 2.5.
3. Using the parametric equation given by 2.4, the position of the planet can be determined. Therefore, the coordinates are  $(x, y, z) = (a \cos(E), b \sin(E), 0)$ . Shift the coordinate system so that the foci  $(ae, 0, 0)$ , where the host star is placed, becomes the new origin. Thus, the final coordinates are

$$(x, y, z) = (a \cos(E) - ae, b \sin(E), 0) \quad (2.9)$$

4. We use  $i, \Omega$  and  $\omega$  as Euler angles and rotate this ellipse to any orientation as specified. This is performed as -
  - (a) Use  $R_z(-\omega)$  to convert the above coordinates in  $xyz$ -system to those of  $x^1y^1z^1$ -system. Let the new coordinates be  $(x^1, y^1, z^1)$ .
  - (b) Use  $R_{x^1}(-i)$  to convert these coordinates in  $x^1y^1z^1$ -system to those of  $x^2y^2z^2$ -system. Let the new coordinates be  $(x^2, y^2, z^2)$ .
  - (c) Use  $R_{z^2}(-\Omega)$  to convert these coordinates in  $x^2y^2z^2$ -system to those of  $XYZ$ -system. Let the new coordinates be  $(X, Y, Z)$ .
5. Since the orbit is seen on the night sky, the view from earth is actually the projection of the position of the planet on the  $xy$ -reference plane. Thus, the coordinates as seen from earth are  $(X_{proj}, Y_{proj}, Z_{proj}) = (X, Y, 0)$ .
6. Calculate the distance between the centres of the host star  $(0, 0, 0)$  and the planet at each value of  $E$ . Use 2.1 to calculate the area of intersection between them.
7. Let the light received from the host star be normalized to 1 unit. When the planet transits across the host star, the light received is equal to  $1 - \frac{A_{intersection}}{A_{star}}$  units. (Here,  $A_{star}$  is equal to  $\pi r_{star}^2$ ). This is because,  $\frac{A_{intersection}}{A_{star}}$  amount of light is blocked by the planet. Thus, a distinctive dip can be seen in the light curve of the star. The curve can be seen in Figure 2.4.

### 2.1.6 Limb Darkening

The intensity of any observed stellar disk is not uniform; it is darker at the edge/limb than at the centre. This effect is called limb darkening. The reduction in the intensity at edge occurs because of the temperature gradient from the core to the surface. The stellar atmospheric thickness and the temperature are very less at edges compared to the rest part of the star. The incoming light coming from the central part comes radially towards us while light coming closer to the limb comes at a slant angle and has to cross longer thickness of a stellar atmosphere.

### 2.1.7 Limb darkening effect in transiting exoplanet

The shape of a light-curve during transit is mainly characterized by the planet to star radius ratio, impact parameter and limb darkening. Thus, an accurate assessment of limb darkening is important while obtaining the transmission spectra and other transit parameters such as planetary radii from the transit data.

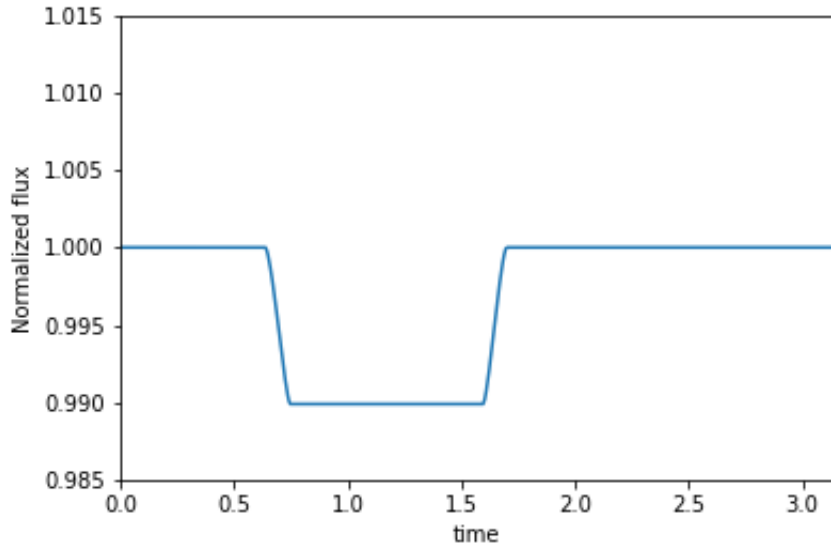


Figure 2.4: Light curve obtained considering a planet with radius approximately 0.1 of the host star. Here, period of the orbit is equal to  $2\pi$  units.  $e = 0.2$ , and  $i = 90^\circ$ ,  $\omega = 0$ ,  $\Omega = 0$ . These parameters have been used for all subsequent plots.

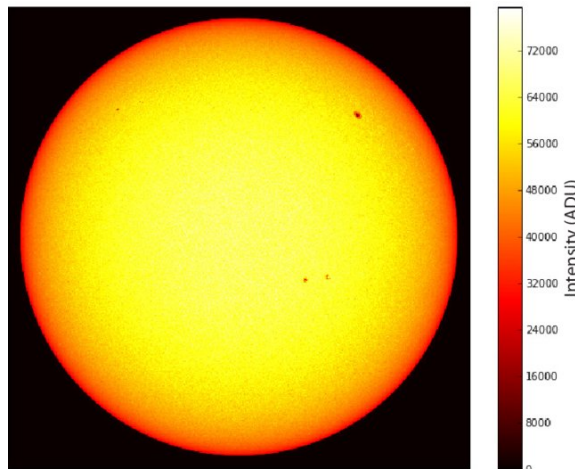


Figure 2.5: Limb darkening of Sun [Moon et al. \(2017\)](#)

Modeling limb darkening is done by several data fitting methods and the solution of radiative transfer equations, based on the stellar atmosphere. Several laws such as the linear law, the quadratic law, the square root law, the logarithmic law, the non-linear law [Claret \(2000\)](#), and the 3-parameters non-linear law [Sing \(2010\)](#) have been proposed in the literature to approximate the intensity variation of the stellar disk. These equations are:

The quadratic law:

$$\frac{I(\mu)}{I(1)} = 1 - a(1 - \mu) - b(1 - \mu)^2$$

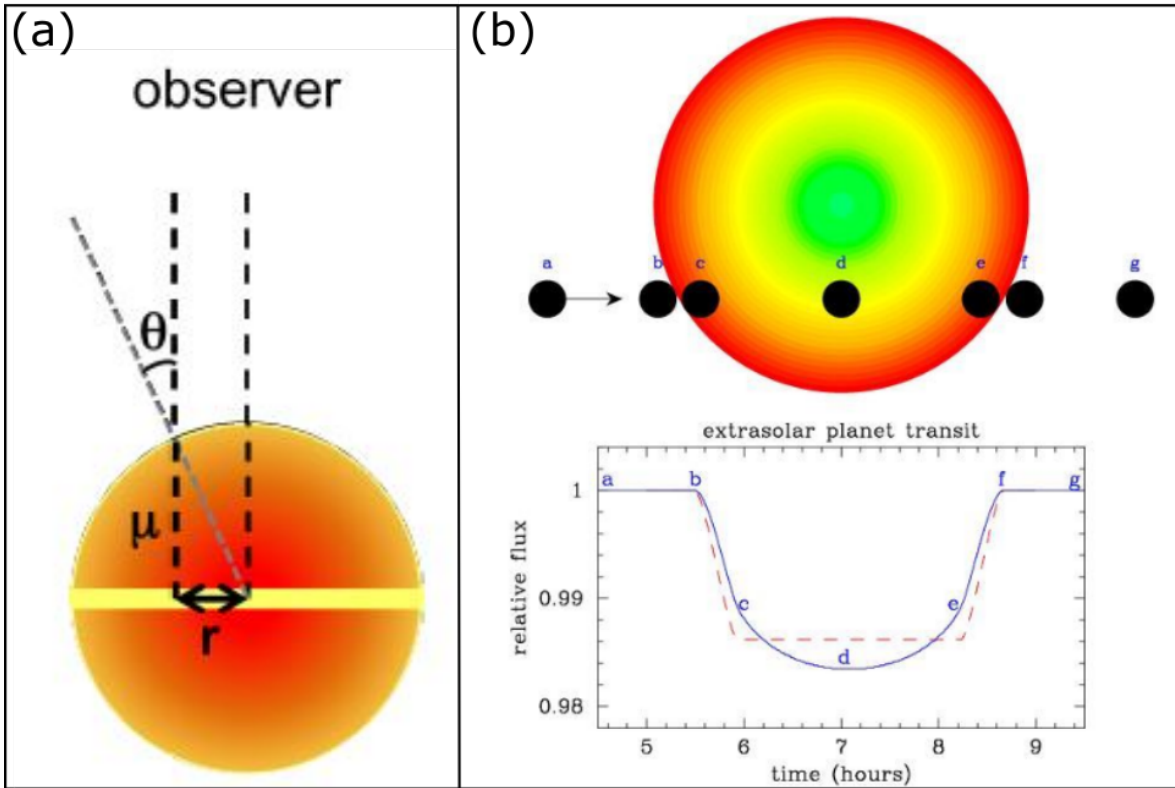


Figure 2.6: (a) geometry of the stellar limb darkening (b) Variation of intensity of a star with and without the effect of limb darkening [Morello \(2016\)](#)

If  $b = 0$ , we get the linear law:

$$\frac{I(\mu)}{I(1)} = 1 - u(1 - \mu)$$

The non-linear law:

$$\frac{I(\mu)}{I(1)} = 1 - c_1(1 - \mu^{1/2}) - c_2(1 - \mu) - c_3(1 - \mu^{3/2}) - c_4(1 - \mu^2)$$

If  $c_1 = 0$ , we get the 3-parameter non-linear law:

$$\frac{I(\mu)}{I(1)} = 1 - c_2(1 - \mu) - c_3(1 - \mu^{3/2}) - c_4(1 - \mu^2)$$

where  $I(1)$  is the intensity at the center of the stellar disk,  $\mu = \cos(\theta)$  (which is the angle between the line of sight and the emergent intensity), while  $u, a, b$ , and  $c_n$  are the Limb darkening coefficients.

The plots of the above 4 equations can be seen below.

Figure 2.7 shows the effect of limb darkening across the disk under various limb darkening laws. This variation depends upon the viewing angle (theta) i.e. angle between the angle between the line-of-sight and the perpendicular to the stellar surface. During transit, the orbiting planet blocks certain flux which varies depending upon the location on the planet in front of the star (using equation

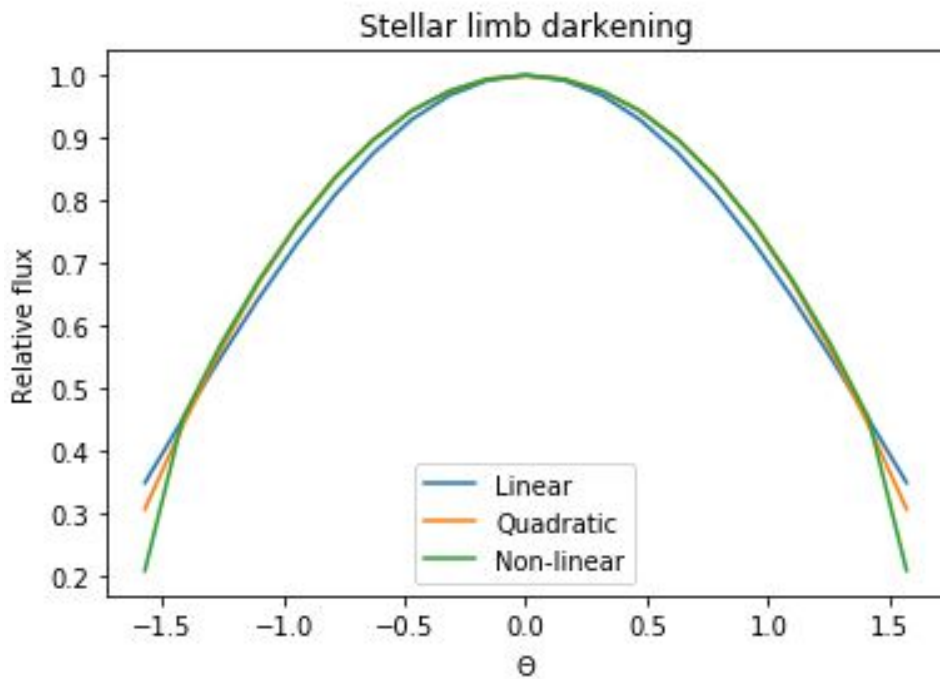


Figure 2.7: Variation of intensity with change in viewing geometry

2.1). This flux is corrected by dividing the unperturbed stellar flux based on limb-darkening laws. Flux of a star is given by:

$$F_* = 1 - \delta' \quad (2.10)$$

$$\delta' = \left[ \int_0^1 I(r) 2\pi(r) (A_{int}) dr \right]^{-1} \left( \int_0^1 I(r) 2\pi(r) dr \right) \quad (2.11)$$

### 2.1.8 Thermal emission and reflected light from exoplanets

1. Thermal emission - The planet get heated by the star and thus emits a thermal flux given by (Schneider (2002)) -

$$F_{th} = \frac{R_{pl}^2}{4a^2} * F_{star}$$

2. Reflected light - The planet reflects the stellar light with a flux ratio given by (Schneider (2002))-

$$F_{th} = \frac{R_{pl}^2}{a^2} * F_{star} * \frac{A_{pl}}{4} * \text{orbital phase factor}$$

Since normalized units are used,  $F_{star} = 1$  units. Also,  $A_{pl}$  refers to the albedo of the planet.

### 2.1.9 Incorporation of limb darkening and other phenomena in the simulation

To make our model more realistic, additional steps can be taken to incorporate limb darkening, thermal emission and reflected light into the simulation. This can be done as follows.

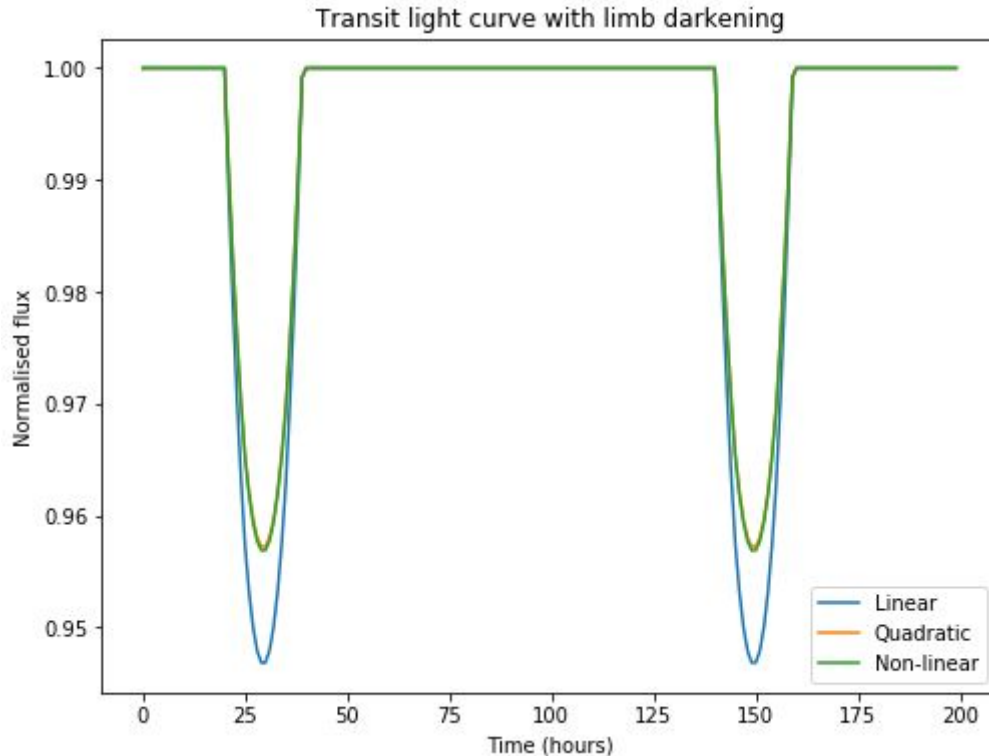


Figure 2.8: A plot to show how different limb-darkening equations might affect the light curve.

- Instead of subtracting  $\frac{A_{\text{intersection}}}{A_{\text{star}}}$  units of light from the normalized 1 units of flux received from the star, subtract  $K * I * \frac{A_{\text{intersection}}}{A_{\text{star}}}$  of the light. Here  $K$  is a constant for the setup, dependent on the relation between  $I$  and flux of the light received from the host star.
- Let the star make an angle of  $x^\circ$  in the night sky. Thus, from the centre of the star to its edge, it makes an angle  $\frac{x}{2}^\circ$ . Since the star is too far away, the angle made can be assumed to be a linear function of the distance from the centre of the star. Thus, at distance 0 from the centre of the star,  $I = I(\mu = 1)$ . At distance  $r_{\text{star}}$  from the star,  $I = I(\mu = \cos(\frac{x}{2}))$ . And at distance  $d$  from the centre,  $I = I(\mu = \cos(\frac{dx}{2r}))$ . Thus using the distance between the centres of the star and the planet calculated earlier, calculate  $I$  at each of those points and use it as mentioned above.
- The light actually seen on earth is also because of thermal emission of the planet and the reflected light from the planet. Thus, we add them to the normalized 1 units of flux received from the star. To add thermal emission, just the factor mentioned above can be used.
- To add reflected light, we calculate the orbital phase factor. When the planet revolves around the star, half of its face is always illuminated. However, if it is at an angle, only a fraction of that light can be seen. This fraction can be calculated as follows -
  - Using the 3D coordinates of the planet and not the projection, calculate the angle made with the  $z$ -axis, the axis perpendicular to the night sky.
  - This is done by taking a dot product and normalizing it, to find  $\cos(\theta)$ . Use this to find theta.

- (c) If the angle is  $0^\circ$ , the planet lies behind the star and thus, its entire reflected light could have reached us (the star blocks the planet's reflected light). If the angle is  $90^\circ$ , half of its entire reflected light reaches us. If the angle is  $180^\circ$ , the planet lies in front of the star and thus, its entire reflected light never reaches us. Thus, for an angle  $\theta^\circ$ , the fraction reaching us is equal to  $1 - \frac{\theta}{180}$ . This is the orbital phase factor.
5. Use the above orbital phase factor and the formula for reflected light, and add it to the light received by the star.

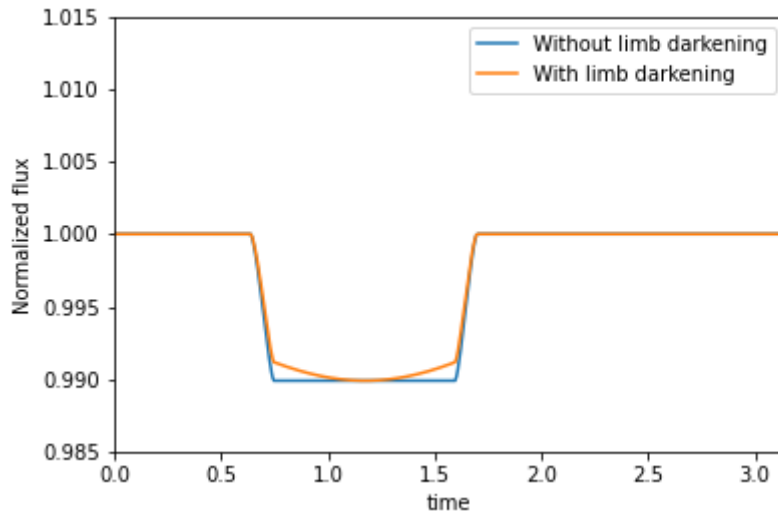


Figure 2.9: Effect of limb darkening. The parameters used for the equation to calculate limb darkening and used for the plot are exaggerated, to give a better visual output. The period of the orbit is  $2\pi$  units.

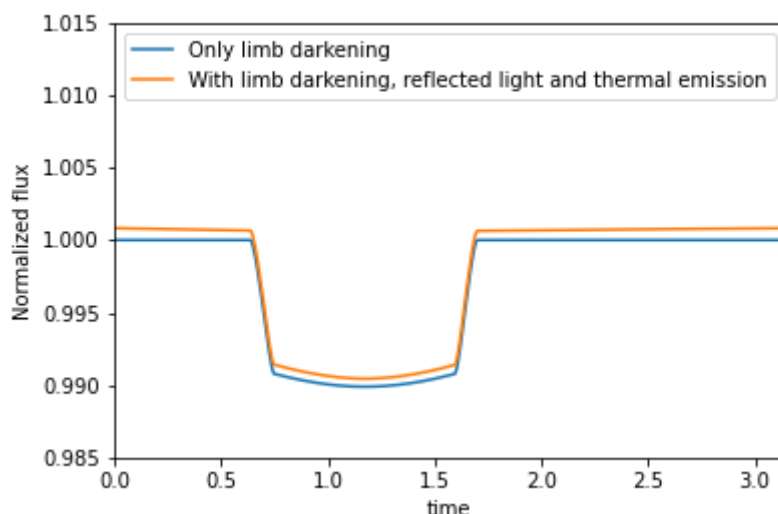


Figure 2.10: Reflected light and thermal emission added to limb darkening. The period of the orbit is  $2\pi$  units.

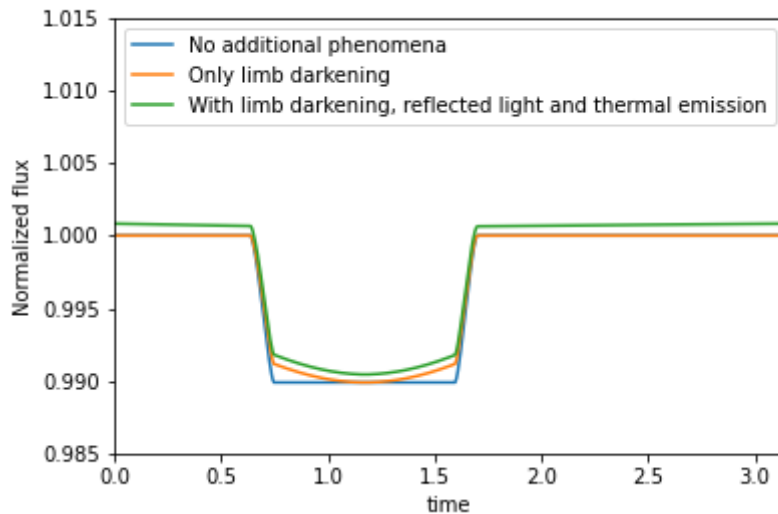


Figure 2.11: All three plots. The period of the plot is  $2\pi$  units.

## 2.2 Radial Velocity

### 2.2.1 Introduction

The radial velocity method also known as Doppler Spectroscopy is used to make Exoplanetary discoveries and it continues to be one of the major tool , the velocity of a star is captured by using the red-shift method . Here we are going to understand the physics behind it and derive necessary equation that govern the light curve .

### 2.2.2 Doppler effect

The fundamental technique on which radial velocity method relies on is the Doppler effect .When the source of the light moves away from the observer, there is a change in the wavelength of light received due to Doppler effect and as the source is moving away we see the red-shift else we see the blue shift

The apparent wavelength is by  $\lambda = \lambda_0 \frac{(1+v/c)}{\sqrt{(1-v^2/c^2)}}$  . The red shift is then given by  $z = \Delta\lambda/\lambda$ .

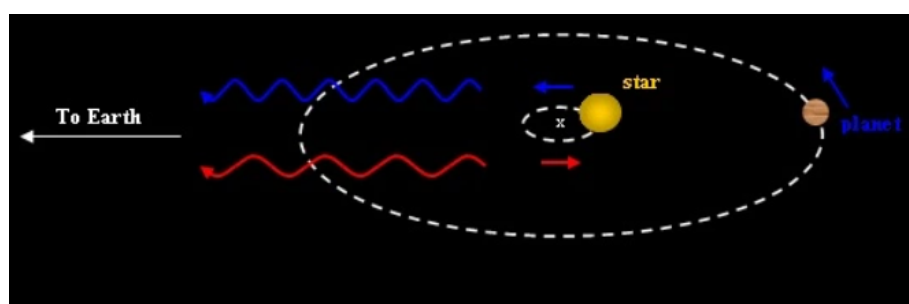


Figure 2.12: Pic credits :Taken from wordpress.com

### 2.2.3 Radial Velocity method

In this method the Radial velocity of the star is captured from Red-Shift data and plotted .When a planet transits in front of the star it blocks the light from the part of star behind it ,as the star is rotating about its own axis half the hemisphere will be red-shifted and half blue-shifted hence when planet transits in front of star it first blocks the red-shifted light and then blue-shifted or vice-versa creating a small perturbation in the graph. Studying this plot we can derive many properties of star planet system

In this section , we will derive the radial velocity equation and also the governing equations of light curve for a star- planet system moving in circular orbits

T = Time period of revolution

a = distance between star and planet

$a_{star}$  = Radius of orbit of star

R = radius of respective bodies

$$a_{star} = a * \frac{M_{planet}}{M_{star} + M_{planet}} \quad (2.12)$$

$$V_{star} = \frac{2\pi a_{star}}{T} \quad (2.13)$$

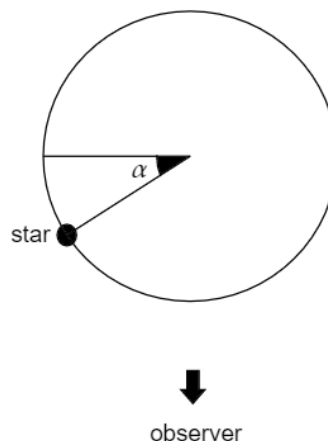


Figure 2.13: Depiction of Star moving around the COM of system

We see from the figure that the velocity directed towards the observer is

$$V_{rad} = V * \cos(\alpha) + V_{COM} \quad (2.14)$$

Plotting this we will see something like this a sinusoidal variation of velocity with time.

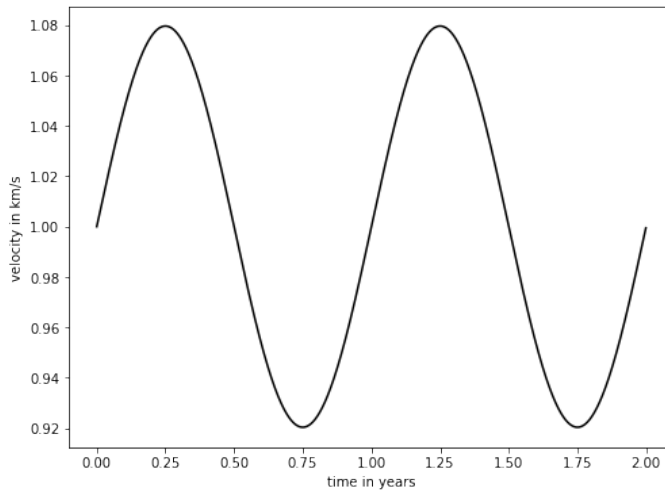
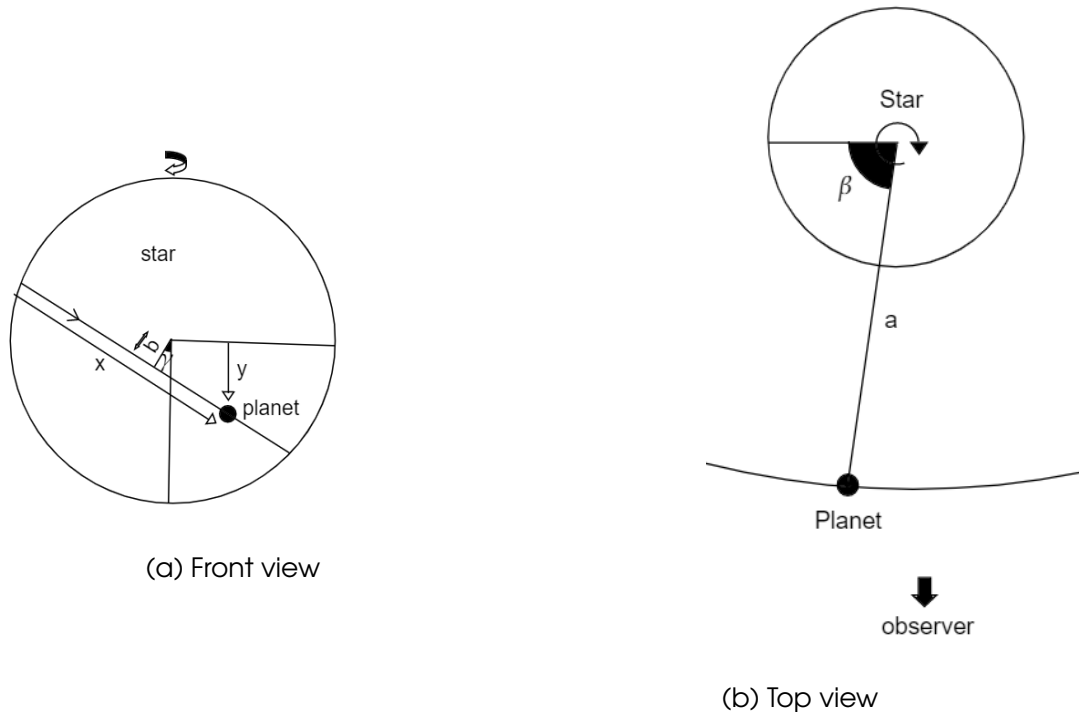


Figure 2.14: Plot of the radial velocity of star with  $V_{COM} = 1\text{km/s}$

Moving further now we calculate the velocity covered by planet when it transits in the plane perpendicular to observers view . For simplicity we assume that radius of planet is very less when compared to radius of star. Taking the axis of rotation of star to be pointing outwards (for figure 1 ) we define an angle  $\beta$  and  $\gamma$  for figure b and a as shown below.



In the figure a we have defined an angle  $\gamma$  (angle marked in the fig a) (tilt of the orbital plane of planet with the star's rotation axis . Now we calculate the velocity of star covered by planet.

$x$  = distance covered along the path

$y$  = vertical distance from equator

$\omega$  = Angular rotation of the star

$\theta$  = Latitude on star

b = Minimum distance between planet path and Star's center.(see fig .a)

$$R_l = \sqrt{(R_{star} + R_{planet})^2 - b^2} \quad (2.15)$$

$$y = (R_l - x) \cdot \sin(\gamma) - b \cdot \cos(\gamma) \quad (2.16)$$

$$\beta = \cos^{-1}\left(\frac{(R_l - x) \cdot \cos(\gamma) + b \cdot \sin(\gamma)}{R_{star} + R_{planet}}\right) \quad (2.17)$$

$$\theta = \sin^{-1}\left(\frac{y}{R_{star} + R_{planet}}\right) \quad (2.18)$$

So now we have all the parameters therefore the velocity curved will be

$$V_{covered} = V_{rotational} + V_{radial} \quad (2.19)$$

$$V_{rotational} = \omega \cdot R_{star} \cdot \cos(\theta) \cdot \cos(\beta) \quad (2.20)$$

$$V_{radial} = V_{star} \cdot \cos(\alpha) \quad (2.21)$$

$$V_{detected} = V_{radial} - V_{covered} \cdot \frac{A_{planet}}{A_{star}} \quad (2.22)$$

Here A is the projected area of the planet and star respectively i.e  $\pi^* r^2$

After adding the Limb darkening correction, the last equation becomes

$$V_{detected} = V_{radial} - V_{covered} \cdot I \cdot \frac{A_{planet}}{A_{star}} \quad (2.23)$$

where I is the relative luminosity at a point covered by planet. Since the luminosity of the star is not same as viewed by observer, we have to use this correction . Having all the equations, we simulated the model and obtained different light curves.

### 2.2.4 Simulation and Plots

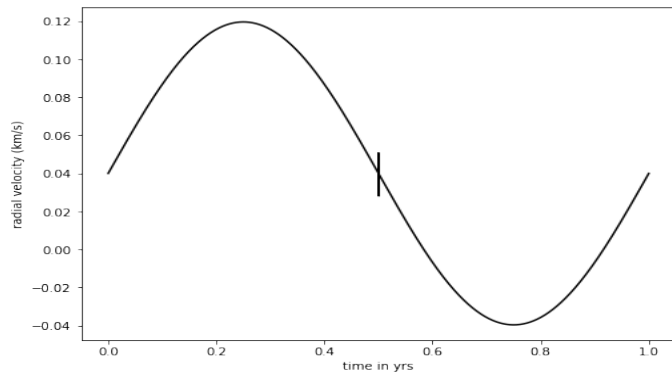


Figure 2.16: Light curve for an entire year is simulated (The values taken are  $R_{planet} = 70000\text{km}$  ,  $R_{star} = 69800\text{km}$  , ratio of masses = 0.001,  $T= 1$  year ,  $a = 40$  million km. the values are similar to that Sun - Jupiter system)

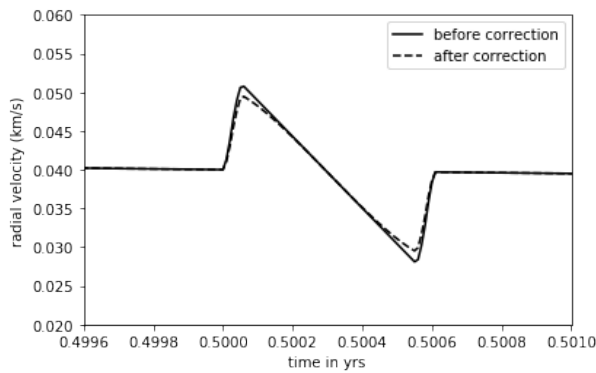
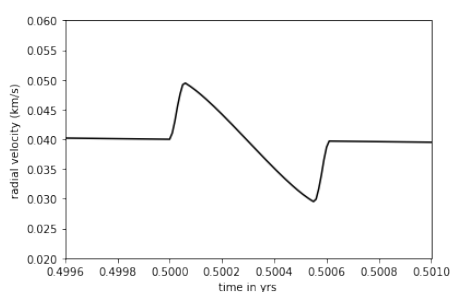
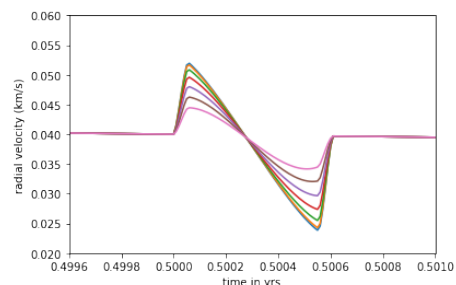


Figure 2.17: Light curve at transit for same parameters as mentioned above we can see the curve plotted before and after limb darkening correction



(a) The Final Light curve at transit after cor-



(b) Light curve for different angular tilt of the orbit of planet ( $\gamma$  varying from 0 to 70 degrees)

### 2.2.5 Radial Velocity Method for an Elliptical Orbit

When a planet orbits a star, its gravitational attraction causes the star to change its radial velocity with respect to the observer. The radial velocity method for exoplanet detection involves recording the oscillations in the Doppler shift of the stellar spectrum due to this change in its radial velocity. In general, only the radial velocity variations of the star are observable, since the flux of the planet is very small compared to that of the star. This method can be used to obtain the orbital period of the planet  $P$ , the eccentricity of its orbit  $e$ , the semi-amplitude of the radial velocity variations of the star  $K_1$ , and the minimum mass  $M_p \sin i$ , if  $(M_p + M_*)$  is known (where  $M_p$  is the mass of the planet,  $M_*$  is the mass of the star, and  $i$  is the angle between the orbital plane and the plane of the sky). Cases where  $i$  is close to  $\pi/2$  are more frequent.

The radial velocity equation is derived in [Lovis & Fischer \(2010\)](#) as follows:

$a_1$  = semi-major axis of the first body orbit around the centre of mass

$a$  = semi-major axis of the relative orbit

$e$  = eccentricity of the orbit

$v$  = true anomaly of the star

$i$  = angle between the orbital plane and the plane of the sky

$\omega$  = angle between line of nodes and periastron direction for the star

$m_1, m_2$  = masses of the bodies

Then,  $a_1$  is related to  $a$  as

$$a_1 = \frac{m_2}{m_1 + m_2} a \quad (2.24)$$

The equation of the ellipse for the first body, in polar coordinates, is

$$\begin{aligned} r_1 &= \frac{a_1(1-e^2)}{1+e \cos v} \\ &= \frac{m_2}{m_1 + m_2} \frac{a(1-e^2)}{1+e \cos v} \end{aligned} \quad (2.25)$$

Now,

$$\vec{r}_1 = \begin{pmatrix} r_1 \cos v \\ r_1 \sin v \end{pmatrix} \quad (2.26)$$

$$\dot{\vec{r}}_1 = \begin{pmatrix} \dot{r}_1 \cos v - r_1 \dot{v} \sin v \\ \dot{r}_1 \sin v + r_1 \dot{v} \cos v \end{pmatrix} \quad (2.27)$$

Also,

$$\begin{aligned} \dot{r}_1 &= \frac{a_1(1-e^2)e\dot{v} \sin v}{(1+e \cos v)^2} \\ &= \frac{er_1^2 \dot{v} \sin v}{a_1(1-e^2)} \end{aligned} \quad (2.28)$$

Substituting this value of  $\dot{r}_1$  in  $\dot{\vec{r}}_1$ ,

$$\begin{aligned} \dot{\vec{r}}_1 &= \frac{r_1^2 \dot{v}}{a_1(1-e^2)} \begin{pmatrix} -\sin v \\ \cos v + e \end{pmatrix} \\ &= \frac{h_1}{m_1 a_1 (1-e^2)} \begin{pmatrix} -\sin v \\ \cos v + e \end{pmatrix} \end{aligned} \quad (2.29)$$

where  $h_1 = m_1 r_1^2 \dot{v}$  is the angular momentum of the first body, and is expressed as a function of  $a$  and  $e$  in Lovis & Fischer (2010) as

$$\begin{aligned} h_1 &= \frac{m_2}{m_1 + m_2} h \\ &= \sqrt{\frac{G m_1^2 m_2^4 a (1 - e^2)}{(m_1 + m_2)^3}} \end{aligned} \quad (2.30)$$

$$\therefore \dot{\vec{r}}_1 = \sqrt{\frac{G m_2^2}{(m_1 + m_2) a (1 - e^2)}} \begin{pmatrix} -\sin v \\ \cos v + e \end{pmatrix} \quad (2.31)$$

The projection of this radial velocity onto the line of sight is required.  
 $\therefore$  the unit vector along the line of sight is

$$\hat{k} = \begin{pmatrix} \sin \omega \sin i \\ \cos \omega \sin i \\ \cos i \end{pmatrix} \quad (2.32)$$

$\therefore$  the required projection

$$\begin{aligned} v &= \dot{\vec{r}}_1 \cdot \hat{k} \\ &= K_1 (\cos(\omega + v) + e \cos \omega) \end{aligned} \quad (2.33)$$

where  $K_1 = \sqrt{\frac{G}{(m_1 + m_2) a (1 - e^2)}} m_2 \sin i$  is the semi-amplitude of the radial velocity variation.

$\because \omega = \omega_p + \pi$  and  $v = v_p + \pi$  (Alapini Odunlade (2010))  
 $\therefore$  where  $\omega_p$  is the angle between line of nodes and periastron direction for the planet, and  $v_p$  is the true anomaly of the planet,

$$\therefore v = K_1 (\cos(\omega_p + v_p) + e \cos(\omega_p + \pi)) \quad (2.34)$$

To plot the radial velocity variation, the true anomaly of the planet should be expressed as a function of time. The expressions mentioned in Alapini Odunlade (2010) have been used for this, and are reproduced here:

M = mean anomaly

P = period of revolution

T = time at the last passage of periastron

E = eccentric anomaly

$$M = \frac{2\pi}{P} (t - T) \quad (2.35)$$

$$M = E - e \sin E \quad (2.36)$$

This equation was solved for E using the Newton-Raphson method. Finally, v is expressed in terms of E using

$$\begin{aligned} \cos v &= \frac{\cos E - e}{1 - e \cos E} \\ \sin v &= \frac{\sqrt{1 - e^2} \sin E}{1 - e \cos E} \end{aligned} \quad (2.37)$$

The expressions for total transit duration  $t_T$  and transit duration with the planet disk fully superimposed on the stellar disk,  $t_F$ , have also been reproduced from [Alapini Odunlade \(2010\)](#):

$$t_T = \frac{P}{\pi} \arcsin \left( \frac{R_*}{a} \frac{\sqrt{(1+R_p/R_*)^2 - ((a/R_*) \cos i)^2}}{\sin i} \right) \quad (2.38)$$

$$\left( \frac{\sin(t_F \pi/P)}{\sin(t_T \pi/P)} \right)^2 = \frac{(1-R_p/R_*)^2 - ((a/R_*) \cos i)^2}{(1+R_p/R_*)^2 - ((a/R_*) \cos i)^2} \quad (2.39)$$

The impact parameter  $b$ , under the approximation  $a \gg R_*$ ,  $t_T \pi/P \ll 1$ , is ([Alapini Odunlade \(2010\)](#))

$$b = \sqrt{\frac{(1-\sqrt{\delta})^2 - (t_F/t_T)^2(1+\sqrt{\delta})^2}{1-(t_F/t_T)^2}} \quad (2.40)$$

where  $R_p$  = radius of the planet,

$R_*$  = radius of the star,

$$\delta = \left( \frac{R_p}{R_*} \right)^2$$

These expressions are for a circular orbit. For planets following an elliptical orbit,  $b$  is multiplied by  $\left( \frac{1-e^2}{1 \pm e \sin \omega} \right)$  ([Alapini Odunlade \(2010\)](#)) ('+' for mid-transit and '-' for mid-occultation). For  $t_T$  and  $t_F$  for an eccentric orbit, a good approximation, mentioned in [Alapini Odunlade \(2010\)](#) is to multiply them by  $\frac{\sqrt{1-e^2}}{1 \pm e \sin \omega}$  ('+' for mid-transit and '-' for mid-occultation.)

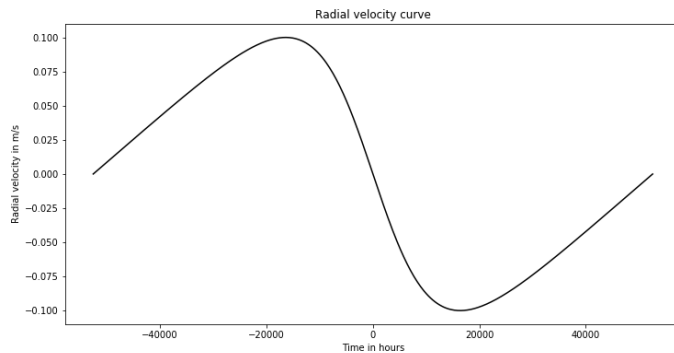


Figure 2.19: Simulated plot for radial velocity variation of a star due to an exo-planet.( $P = 12$  years,  $e = 0.3$ ,  $K_1 = 0.1$ ,  $\omega = 3\pi/2$ ,  $i = \pi/2$ )

### Rossiter-McLaughlin Effect

For a rotating star, the observer sees the hemisphere moving towards them as blue-shifted, and the hemisphere moving away as red-shifted. When a planet transits the star, the average flux received by the observer is shifted towards the blue or red end, depending on whether the planet is covering the red-shifted or the blue-shifted side, respectively. Thus, the radial velocity of the star, which is measured using the Doppler shift of the star, appears to change too. This effect lasts for the entire transit.

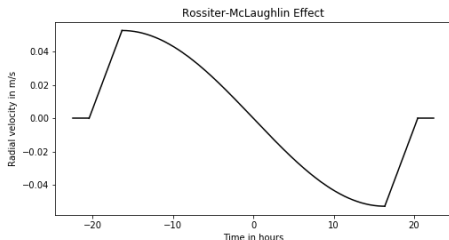
Here, the Rossiter-McLaughlin effect has been simulated as a sinusoidal curve to include the limb darkening of the star. The semi-amplitude of this curve is mentioned by [Triaud \(2017\)](#):

$$A = \frac{2}{3} \delta v \sin i_* \sqrt{1 - b^2} \quad (2.41)$$

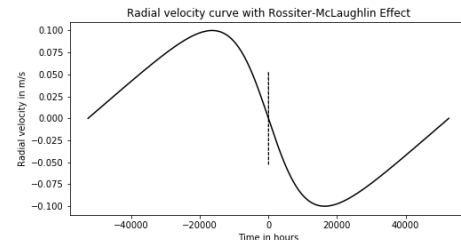
where  $\delta = \left(\frac{R_p}{R_*}\right)^2$ ,

$v$  = rotational velocity of the star at the equator,

$\sin i_*$  = inclination of the stellar rotation axis on the sky.



(a) Simulated plot for Rossiter-McLaughlin effect for a transiting planet in an elliptical orbit.



(b) Simulated radial velocity variation of a star due to an exoplanet, with the Rossiter-McLaughlin effect incorporated.

Figure 2.20: Exaggerated values have been taken.  $P = 12$  years,  $R_p = 69911$  km,  $R_* = 627938$  km, semi-major axis of orbit  $a = 778$  million km,  $e = 0.3$ ,  $\omega = 3\pi/2$ ,  $v = 0.0065$  m/s,  $K_1 = 0.1$ ,  $i = \pi/2$ ,  $i_* = \pi/2$

## 2.3 Gravitational Lensing

### 2.3.1 Introduction

One of the consequences of Einstein's General Theory of Relativity is that light rays are deflected by gravity. This deflection of light by massive bodies, and the phenomena resulting therefrom is known as Gravitational Lensing. Gravitational microlensing refers to the special case when multiple images are created but have very less separation which is unresolved with current technology resulting in an observable magnification of the source star. The lens passes by the source in a reasonable amount of time. As the alignment of the lens with respect to the source changes, the apparent brightness of the source changes. Studying this lensing effect caused by heavy masses can give us an insight into the properties of the lens. Thus gravitational microlensing is being used to study properties of dark matter, detect exoplanets etc.

When the lens is composed of more than one object, we see that the light curve is not smooth and exhibits sharp spikes which depends on relative masses between objects. Studying the light curve, different systems like binary stars and star-planet systems can be detected.

### 2.3.2 Theory

In this section, we will study more about the phenomenon of gravitational lensing. The deflection of light by a massive object is explained by General Theory of Relativity. According to the theory, light follows a geodesic i.e. a straight line path in flat spacetime. As massive objects warp spacetime, the light is bent towards the mass. This bending gives rise to some interesting phenomena:

- Multiple paths around the lens (massive object) are possible resulting in multiple images of a single source (closer images are unresolved and appear to be a single image).
- The ray of light closer to the lens get deflected more than the rays that are farther away.
- Since the number of photons reaching us is the same from the source (photons are neither created nor destroyed) the image just gets magnified or demagnified.
- Due to multiple paths, the travel time is also different for different images and since the astronomical lengths are great, we observe time delays between images.

Now we take a classical approach and consider only weak lenses (those lens having Newtonian potential  $\phi \ll c^2$ ) and try to find the deflection of light rays by a mass  $M$  and minimum approach distance  $b$ . We know by Newtonian gravity that:

$$\mathbf{a} = \frac{GM}{r^3} \cdot \mathbf{r} \quad (2.42)$$

$$r = \frac{b(1+e)}{1 + e \cos(\phi)} \quad (2.43)$$

$$v^2 = \frac{GM}{b(1+e)} (1 + 2e \cos(\phi) + e^2) \quad (2.44)$$

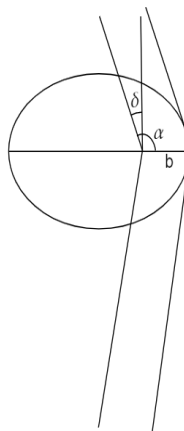


Figure 2.21: Classical approach

Applying these equation to a photon we take  $r \rightarrow \infty$  and  $v \approx c$ . From equation 2, we get  $\cos(\alpha) = -\frac{1}{e}$  and  $v = c$ , rewriting  $\alpha = 90 + \delta$  (see fig below), we obtain:

$$e = \frac{bc^2}{GM} + 1 \quad (2.45)$$

Thus we find the deflection angle  $\alpha \approx 2\delta \approx \frac{2GM}{b*c^2}$

The actual deflection from General Theory of Relativity comes out to be around twice the value obtained from the classical one. The approach to find the deflection angle is to obtain the refractive index as a function of potential ( $\phi$ ) Meneghetti (2006). The light travelling close to the gravitational lenses in a locally Minkowskian spacetime perturbed by the potential is given by

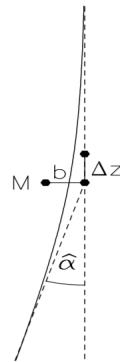
$$n = 1 - 2 \frac{\phi}{c^2} \quad (2.46)$$

where  $\phi$  is the Newtonian gravitational potential i.e

$$\phi(b, z) = -\frac{GM}{\sqrt{b^2 + z^2}} \quad (2.47)$$

where  $b$  is the impact parameter and  $z$  is the distance along the unperturbed path of light from the closest approach as shown in the figure. The angle of deflection is given by Ramesh Narayan (1997):

$$\hat{\alpha} = \frac{2}{c^2} \int_{-\infty}^{\infty} \nabla_{\perp}(\phi) dz \quad (2.48)$$



For a simple point lens system, the deflection angle Meneghetti (2006) comes out to be,

$$\hat{\alpha} = \frac{4GM}{bc^2} \quad (2.49)$$

### Lens Equation

In the figure we sketch a simple gravitational lens system for a point source.

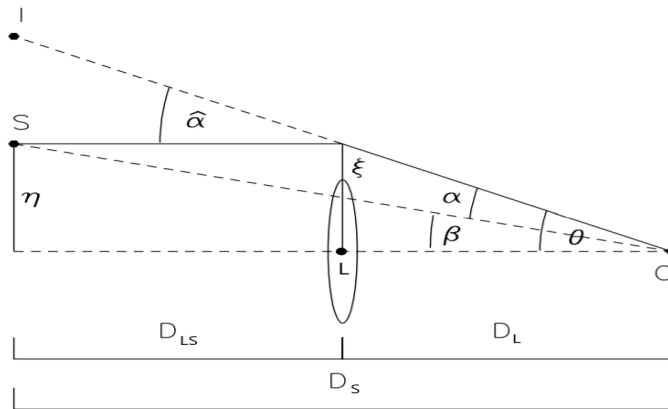


Figure 2.22: Lens diagram

We define an optical axis defined by the dashed line through the lens (L) at the bottom. The original position of the source is at angular position  $\beta$ . Due to the

lensing the observer sees the source at position  $\theta$ . Here  $\hat{\alpha}$  is the angle of deflection. All the angles are very small hence small angle approximation is valid. From the figure :

$$\theta D_S = \beta D_S + \hat{\alpha} D_{LS} \quad (2.50)$$

Defining

$$\alpha(\theta) = \hat{\alpha} \frac{D_{LS}}{D_S} \quad (2.51)$$

$$\beta = \theta - \frac{4GM}{bc^2} \frac{D_{LS}}{D_S} \quad (2.52)$$

Here  $\hat{\alpha} = \frac{4GM}{bc^2}$ , where b is the impact parameter. From Figure we see that  $b = \theta D_L$ . Substituting these back into equation 8, we get

$$\beta = \theta - \frac{\theta_E^2}{\theta} \quad \text{where,} \quad \theta_E = \left( \frac{4GM}{c^2} \frac{D_{LS}}{D_S D_L} \right)^{1/2} \quad (2.53)$$

Taking  $\frac{\beta}{\theta_E} = y$  and  $\frac{\theta}{\theta_E} = x$ , we get an equation  $y = x - \frac{1}{x}$ . Thus for every y, there are two solutions for x, therefore for a point lens two images are formed for every source position of y. Solving the above equation we get

$$x \pm = 0.5[y \pm \sqrt{y^2 + 4}] \quad (2.54)$$

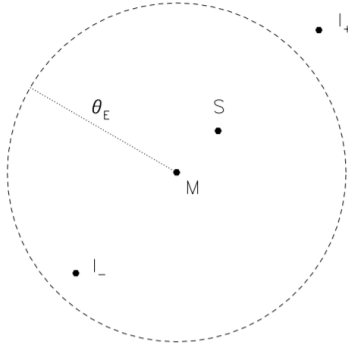


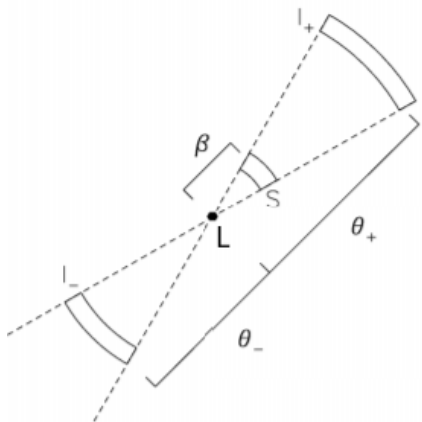
Figure 2.23: Images and source

$\theta_E$  is called the Einstein radius. The Einstein radius is a natural angular scale to describe the lensing geometry . If there are multiple sources, the sources which are closer than about  $\theta_E$  to the optic axis experience strong lensing which means they are significantly magnified, whereas sources which are located well outside the Einstein ring are magnified very little.

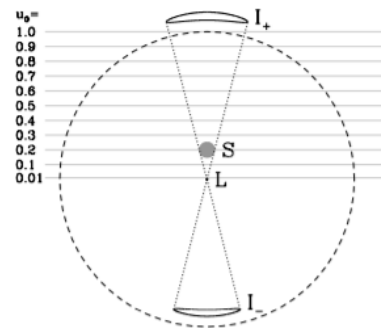
### Magnification

Due to the phenomena of Gravitational Lensing the images are distorted and also magnified. However the gravitational deflection of light preserves the surface brightness ( Liouville's Theorem). Thus the total flux received from the images and source is proportional to the surface area.

$$\text{Magnification} = \frac{\text{image area}}{\text{source area}} \quad (2.55)$$



(a) Magnification of images



(b) Einstein Ring, source and its images

Considering it to be a lens with circular symmetry, the magnification for an image can be written as (see Figure a )

$$\text{Magnification}(m) = \frac{\theta}{\beta} \frac{d\theta}{d\beta} \quad (2.56)$$

The total magnification can be written as the sum of the individual magnifications of all the images, in the case of a point source:

$$m = m_1 + m_2 \text{ for the two images obtained} \quad (2.57)$$

### 2.3.3 Simulation

#### Equations used

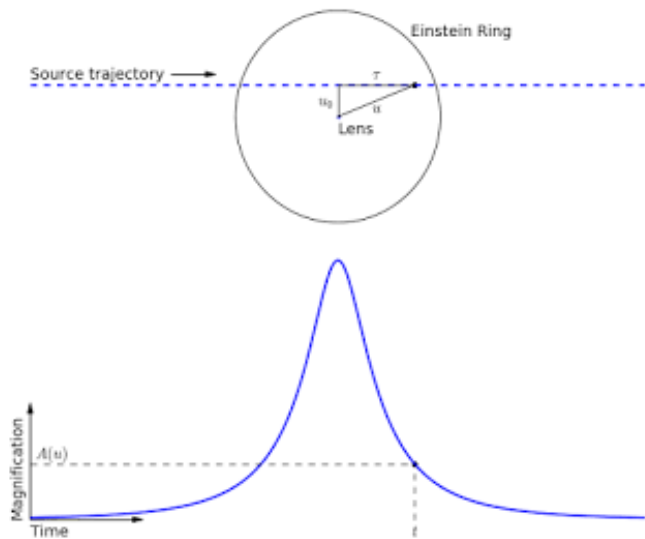


Figure 2.25: Parameters involved.([microlensing source.org \(2017\)](#))

The expressions used for the simulations have been taken from [microlensing source.org \(2017\)](#):

$u_0$  = impact parameter between the source and the lens

$t_0$  = time of closest approach between the source and the lens (i.e. when  $u = u_0$ )

$t_E$  = time for the source to travel one Einstein radius

Then, the magnification of the source is

$$A = \frac{u^2 + 2}{u(u^2 + 4)^{1/2}} \quad (2.58)$$

where,

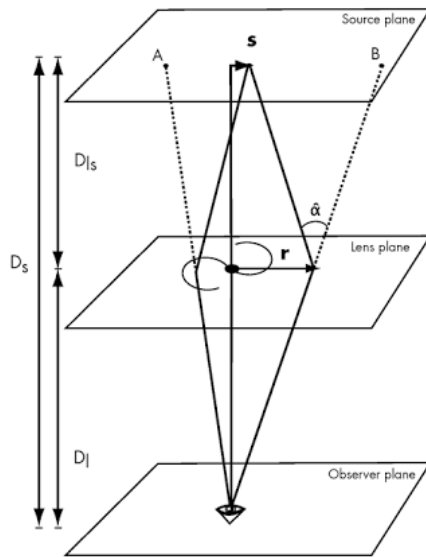
$$u = (u_0^2 + \tau^2)^{1/2} \quad (2.59)$$

$$\tau = \frac{t - t_0}{t_E} \quad (2.60)$$

The Einstein radius was calculated using the following expression, taken from [Meneghetti \(2006\)](#):

$$r_E = \left( \frac{4GM_*}{c^2} \frac{D_L D_{LS}}{D_S} \right)^{1/2} \quad (2.61)$$

where  $G$  is the Gravitational constant,  $c$  is the speed of light,  $M_*$  is the mass of the lensing star, and  $D_L$ ,  $D_{LS}$  and  $D_S$  have been defined in the following diagram ([Elíasdóttir et al. \(2006\)](#)):

Figure 2.26:  $D_{LS}$ ,  $D_S$  and  $D_L$ 

If the relative velocity between the source and the lens is  $v$ ,

$$\begin{aligned} t_E &= \frac{r_E}{v} \\ &= \frac{1}{v} \left( \frac{4GM_*}{c^2} \frac{D_L D_{LS}}{D_S} \right)^{1/2} \end{aligned} \quad (2.62)$$

Thus, the duration of the event is proportional to the square root of the mass of the lens.

$\therefore$  if the time taken to cross one Einstein radius is  $t_{E,p}$  for the planet and  $t_{E,*}$  for the parent star, then

$$\frac{t_{E,p}}{t_{E,*}} = \left( \frac{M_p}{M_*} \right)^{1/2} \quad (2.63)$$

where  $M_p$  is the mass of the planet.

### Plots

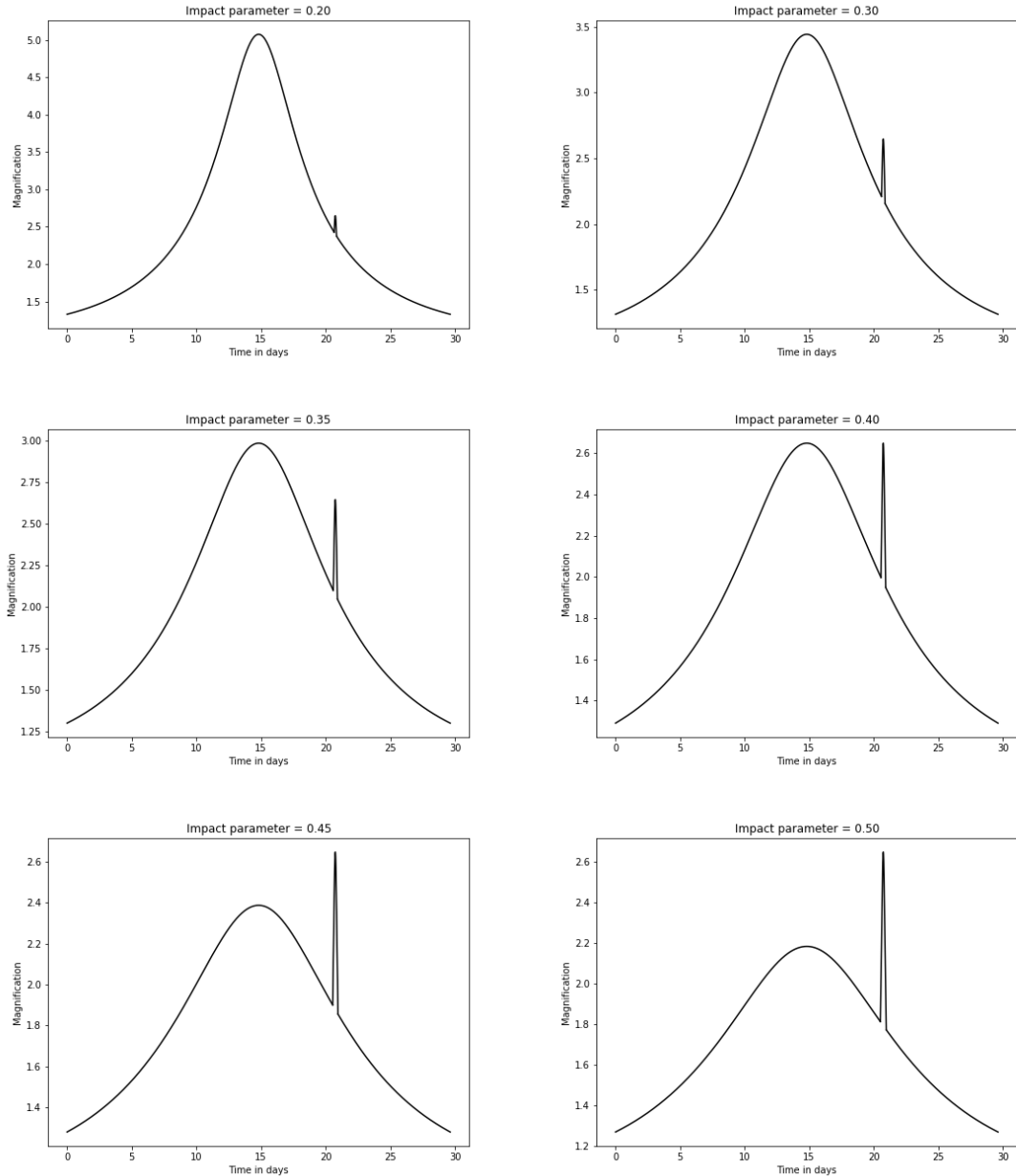


Figure 2.27: Simulated plots for a microlensing event ( $M_* = 1.989 \times 10^{30}$  kg,  $M_p = 1.898 \times 10^{27}$  kg,  $D_L \approx D_S \approx D_{LS} \approx 10$  kpc,  $v = 6 \times 10^5$  m/s) for different impact parameters of the lensing host star. As the impact parameter increases, i.e., as the minimum distance between the source and the lensing star increases, the curve becomes flatter.

## 2.4 Direct Imaging

Direct Imaging as the name suggests involves capturing of the images directly using different filters. Planets are extremely faint objects when compared to stars

and hence will be lost in the glare of star. So they are detected by thermal emission (infrared wavelengths). Usually stars are billion times more brighter than planets but by filtering only infrared radiation the ratio reduces to about a million.

The opportunities for using this method is rare and to detect earth-sized planet is extremely difficult and also for the star-planet system which are very far from us. It becomes relatively easier to capture when the planet is large and widely separated from it's star. Coronagraphs are used to block the light coming from star while leaving that of the planet which makes it easier to detect and analyze the planets . Many other imaging techniques are used to resolve and study the captured images

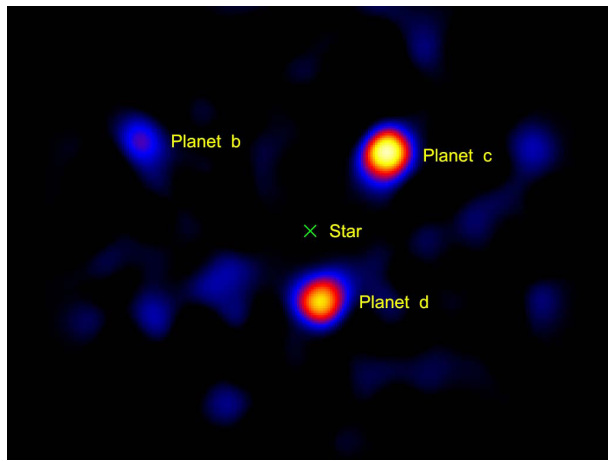


Figure 2.28: Here coronagraph is used to block star's light and only planets light is being captured. Image credit: NASA/JPL-Caltech/Palomar Observatory

While opportunities are rare ,if an exoplanet is detected using Direct Imaging technique it can provide valuable information of planet. By examining the spectra reflected from a planet's atmosphere, astronomers are able to obtain vital information about its composition. It can be used to accurately measure the planet's orbit around the star. The Direct Imaging technique is limited by technology, in future with better telescopes and other instruments we will be able to widen the scope of this method.

## 2.5 Pulsar Timing

Pulsars are usually born out of supernova explosions of massive stars, and are stable cosmic clocks. A major part of the electromagnetic wave emission from pulsars is due to magnetic dipole radiation. This causes them to lose rotational energy and therefore leads to a decrease in their spin frequency. The surface magnetic field strength for a pulsar is usually of the order of  $10^{12}$  G, with spin periods ranging from 0.1 to 1.0 s. Millisecond pulsars, on the other hand, have smaller periods (of the order of a few milliseconds), and surface magnetic field strengths ranging from  $10^7$  to  $10^{10}$  G ([Kramer \(2018\)](#)).

The pulses emitted are dispersed when travelling through the inter-stellar medium,

on their way to the earth. The pulses received are corrected for such dispersions and processed to obtain the time of arrival. This is compared to the predictions of a timing model that includes all the relevant parameters. The deviations from the model are minimized using a least-squares fit for the parameters, to obtain the post-fit residuals.

If the pulsar has a companion, such as a planet, it will cause a reflex motion of the pulsar, leading to variations in the arrival time of the pulses. This, in turn, leads to deviations in the post-fit residuals.

If the orbital period of the companion  $P$  is less than the observing span  $T$ , this induces a periodic variation of the residuals. If  $P$  is larger than  $T$ , a part of the signals is absorbed in fits for the spin frequency  $\nu$ , its first-order derivative  $\dot{\nu}$  and the spin phase, while the movement and acceleration of the pulsar due to the companion are evident in higher-order derivatives of  $\nu$ .

The first exoplanets were detected using this technique in 1992, when [Wolszczan & Frail \(1992\)](#) discovered the presence of atleast two planets (with masses 2.8 and 3.4 times the mass of the earth, and with orbital periods of 98.2 and 66.6 days respectively) around the millisecond pulsar PSR1257+12.

## 2.6 Conclusion

Although the main methods given here have been used for the successful detection of several exoplanets, each has its own limitations that could be addressed for the improved detectability of exoplanets.

False detections of extrasolar planets might be caused by small stars and brown dwarfs, which are comparable in size to gas giants and therefore produce nearly the same depth in the transit lightcurve. However, their masses are usually different, so they could be distinguished using the radial velocity method. Grazing binaries too produce lightcurves with comparable depths, although they produce V-shaped curves, while those of transiting exoplanets have a characteristic U-shape. Colour photometry can also be used to distinguish stellar systems from planets.

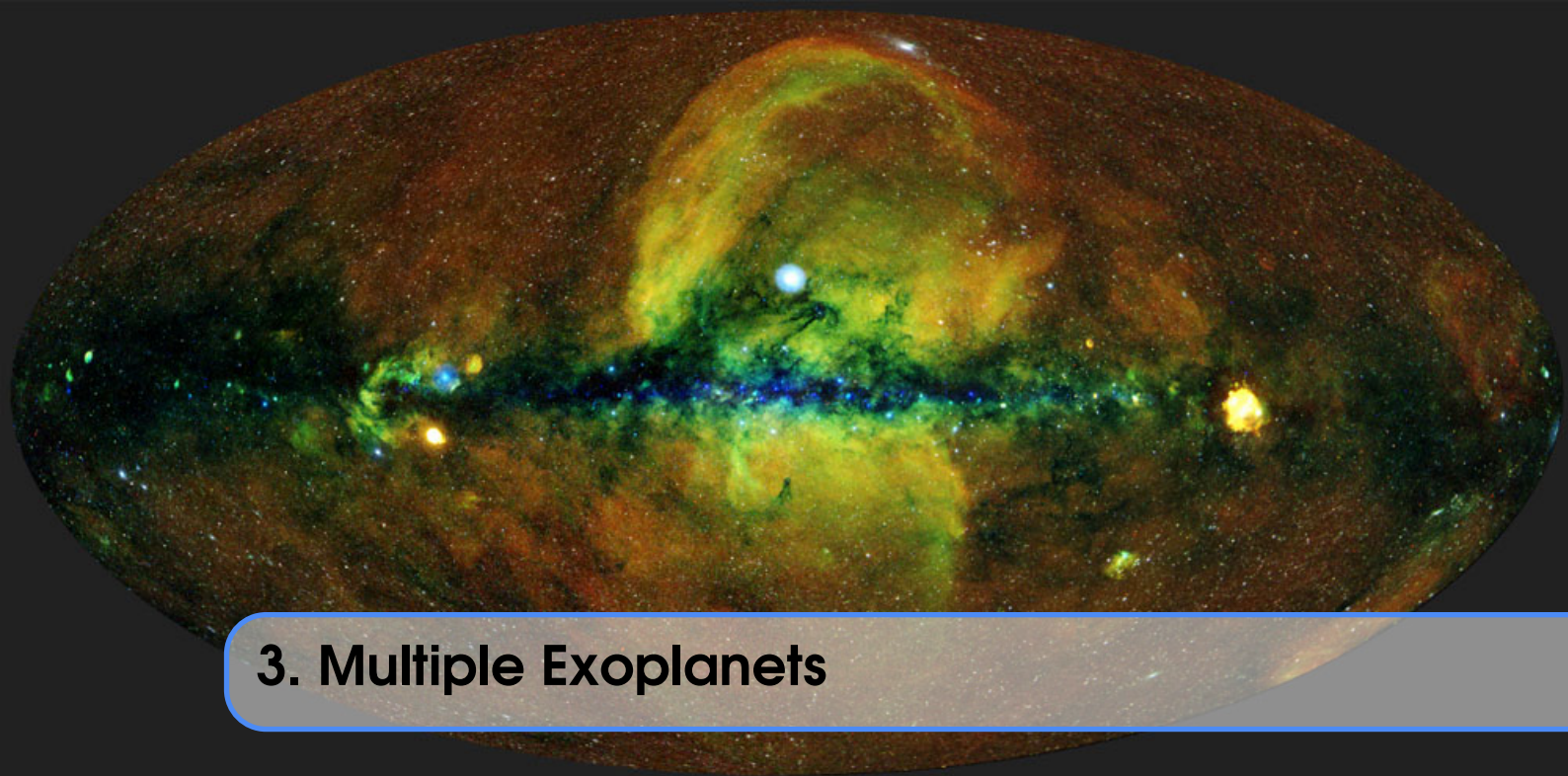
Both the transit and the radial velocity methods could be hampered by stellar activity, such as the variation of magnetic field lines (more common in younger stars), stellar granulations and stellar oscillations. These effects may have larger amplitudes than those produced by planets, and are therefore capable of creating spurious signals.

Noise caused by instrumental or atmospheric effects, such as the changing refractive index of the air, reduce detectability of exoplanets. Other sources of noise in the radial velocity method include temperature changes of the components of the spectrograph, variations in slit illumination, the want of an ideal calibration source, and spurious radial velocity signals from the Earth's atmosphere, moonlight and other sources.

While microlensing is the only method for detecting exoplanets at very large distances, these are unique and unpredictable events and cannot be used to detect the same exoplanet twice. Besides, the distance from the Earth to the lensing system is only approximately known.

With the direct imaging method, it is difficult to detect the light of the planet using current technology, due to the much greater brightness of the parent star. It is also usually effective only for planets that are massive or far from their parent star.

Pulsar timing is extremely precise and can detect objects as small as asteroids, but very few exoplanets have been detected using this method, for reasons not yet fully clear.



## 3. Multiple Exoplanets

### 3.1 New Approach to Transit Light Curve

Sections 2.1 and 4.1 describe two different approaches of Transit Light Curve. Extending either of these approaches to a system consisting of multiple exoplanets orbiting a single star is not possible (at least computationally).

The reasons being:

1. The first approach described in Section 2.1 uses the overlap of the area between the planet and star. However in our case, we would have many planets and thus, have to calculate total area of overlap by applying set theory over multiple areas of overlap. This would be computational heavy especially when the number of planets is large.
2. The second approach described in Section 4.1 finds the the length of the transit period and accordingly calculates the dip in luminosity. But during the transit, two planets might have common areas of shadow which can not be accounted for here.

Thus, we resort to a approach which is inspired from the first approach but instead of using overlap of areas, we use the imaging method.

The approach in brief consists of the following steps:

1. Finding the true anomaly (angle between the direction of periastron and the current position of the body, as seen from the main focus of the ellipse) w.r.t time from the last periastron.
2. Using the true anomaly to find the position of the planet as seen by the observer (in our case, Earth)
3. Calculating the luminosity using imaging method.

This approach is keeping in mind that we have computational powers at our hand.

### 3.1.1 Finding the True Anomaly

Like Section 1.1, we use Kepler's Laws but in a slightly different way.

We form a differential equation which on solving gives us the relation between the True anomaly (henceforth referred as  $\alpha$ ) and time.

Stating Kepler's Second Law, or The Law of Equal Areas in Equal Time -

*The line between a planet and the sun sweeps out equal areas in the plane of the planet's orbit over equal times.*

With  $r$  being the distance between the star and the planet and  $\alpha$  being the true anomaly, the law can be written as the following differential:

$$\frac{1}{2} r^2 \frac{d\alpha}{dt} = \text{constant (say } k\text{)} \quad (3.1)$$

Let  $P$  be the period of revolution of the planet around star.

$$\int_0^{2\pi} \frac{1}{2} r^2 d\alpha = \int_0^P k dt = \text{Area of ellipse} \quad (3.2)$$

We know that the area of the ellipse is  $\pi ab$ . ( $a$  and  $b$  are length of semi-major and semi-minor axis)

We get that  $k$  as  $\frac{\pi ab}{P}$ .

Re-writing Equation 3.1,

$$\frac{d\alpha}{dt} = \frac{2\pi ab}{Pr^2} \quad (3.3)$$

Using the properties of ellipse, we write  $r$  and  $b$  in terms of  $\alpha$  and  $a$ .

$$r = \frac{a(1-e^2)}{1+e\cos(\alpha)} \quad (3.4)$$

$$b = a\sqrt{1-e^2} \quad (3.5)$$

Using Equations 3.3, 3.4 and 3.5

$$\frac{d\alpha}{dt} = \frac{2\pi b \cdot (1+e\cos(\alpha))^2}{P \cdot a(1-e^2)^2} \quad (3.6)$$

$$\frac{d\alpha}{dt} = \frac{2\pi \cdot (1+e\cos(\alpha))^2}{P \cdot (1-e^2)^{1.5}} \quad (3.7)$$

We have derived a differential relation between  $\alpha$  (the true anomaly) and time, with known parameters being  $P$ , the period of revolution and  $e$ , eccentricity.

### 3.1.2 Finding position of the Planet

We need to find the position of the planet given the true anomaly,  $\alpha$ .

Each orbit is uniquely defined by  $a$  (semi-major axis),  $i$  (inclination),  $e$  (eccentricity) and  $\omega$  (periastron angle).

We already have a relation between  $r$  and  $\alpha$  from Equation 3.4. Now on, we would refer  $r$  as  $r(\alpha)$ .

We need to incorporate inclination ( $i$ ) of the orbit w.r.t. the normal sky plane and the argument of periastron ( $\omega$ ) of the planet's orbit (i.e. the position angle of the periastron from the ascending node).

Looking onto the orbit normally with the periastron on +ve x-axis.

$$\begin{bmatrix} x \\ y \\ z \end{bmatrix} = \begin{bmatrix} r(\alpha) \cdot \cos(\alpha) \\ r(\alpha) \cdot \sin(\alpha) \\ 0 \end{bmatrix} \quad (3.8)$$

Now, rotating the coordinate system by  $\omega$  about z-axis.

$$\begin{aligned} \begin{bmatrix} x \\ y \\ z \end{bmatrix} &= \begin{bmatrix} \cos(\omega) & -\sin(\omega) & 0 \\ \sin(\omega) & \cos(\omega) & 0 \\ 0 & 0 & 1 \end{bmatrix} \begin{bmatrix} r(\alpha) \cdot \cos(\alpha) \\ r(\alpha) \cdot \sin(\alpha) \\ 0 \end{bmatrix} \\ &= \begin{bmatrix} r(\alpha) \cdot (\cos(\alpha) \cdot \cos(\omega) - \sin(\alpha) \cdot \sin(\omega)) \\ r(\alpha) \cdot (\cos(\alpha) \cdot \sin(\omega) + \sin(\alpha) \cdot \cos(\omega)) \\ 0 \end{bmatrix} \\ &= \begin{bmatrix} r(\alpha) \cdot (\cos(\alpha + \omega)) \\ r(\alpha) \cdot (\sin(\alpha + \omega)) \\ 0 \end{bmatrix} \end{aligned} \quad (3.9)$$

Rotate the coordinate system by  $i$  about x-axis to incorporate inclination.

$$\begin{aligned} \begin{bmatrix} x \\ y \\ z \end{bmatrix} &= \begin{bmatrix} 1 & 0 & 0 \\ 0 & \cos(i) & -\sin(i) \\ 0 & \sin(i) & \cos(i) \end{bmatrix} \begin{bmatrix} r(\alpha) \cdot (\cos(\alpha + \omega)) \\ r(\alpha) \cdot (\sin(\alpha + \omega)) \\ 0 \end{bmatrix} \\ &= \begin{bmatrix} r(\alpha) \cdot (\cos(\alpha + \omega)) \\ r(\alpha) \cdot (\sin(\alpha + \omega)) \cdot \cos(i) \\ r(\alpha) \cdot (\sin(\alpha + \omega)) \cdot \sin(i) \end{bmatrix} \end{aligned} \quad (3.10)$$

We now have a relation between the coordinates of the planet as seen by the observer in terms of  $\alpha$ .

### 3.1.3 Imaging Method to calculate luminosity

Until now we have dealt with each planet separately.

The only two approximations which we are going to consider are:

1. The star is massive enough to show minimal motion, i.e., the center of the system is close to center of the star.  
This is a fair assumption given that most of the mass of a planetary system lies in the star.
2. The luminosity due to planets reflecting star's light is insignificant, i.e., the dip during occultation is minute as compared to the dip during transit.  
This assumption is fair as the dip in the luminosity caused by occultation is less than the measuring capacity of most of the detectors known.

Method:

- We divide the star into an  $n \times n$  array with each data point equivalent to a pixel.
- The pixels detecting the light from star are given 0 or 1 as value.
- To incorporate limb darkening, we multiply the value of each pixel with the factor of limb darkening using any of the laws stated in Section 2.1.7.
- Now, we have the image of the star when none of the exoplanets are transiting.

- With the position of planets known w.r.t. the center of the star, we can determine their position on the array.
- Taking one planet at a time, we change the value of the pixels it covers to 0.
- This way we don't have to consider different cases of whether the planet is between 1st and 2nd touch, or 2nd and 3rd touch, or 3rd and 4th touch.
- We also don't have to separately consider overlap of shadows of multiple planets as they are causing dip of the luminosity in only those pixels which are already lit up.
- The greater the value of  $n$ , more accuracy we get in the light curve.

## 3.2 Plots

### 3.2.1 True Anomaly Vs Time

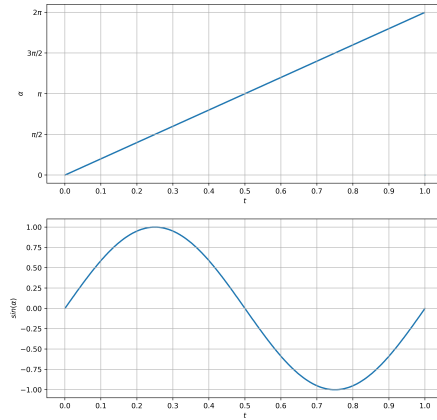
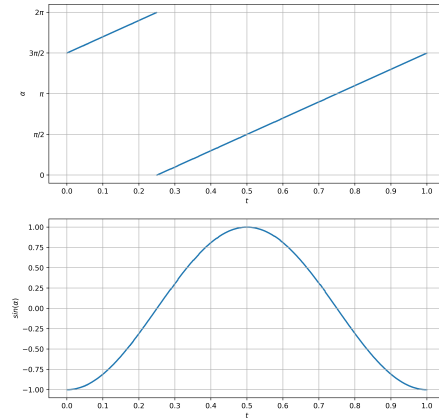
(a)  $e = 0.0$  and  $t_0 = 0.0$ (b)  $e = 0.0$  and  $t_0 = 0.25$ 

Figure 3.1: Circular orbit

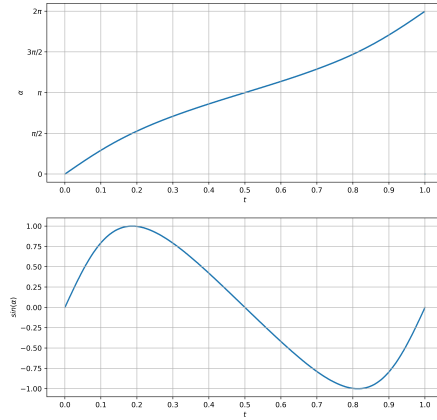
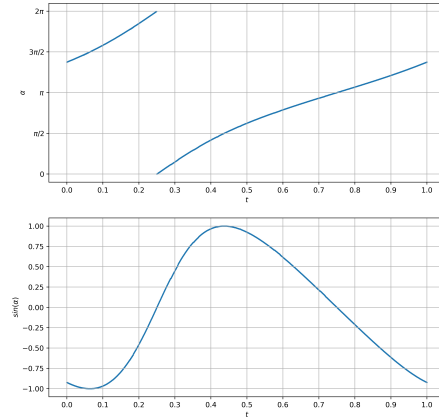
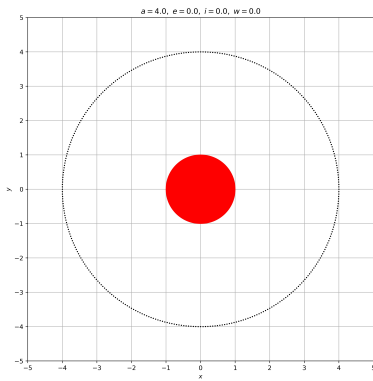
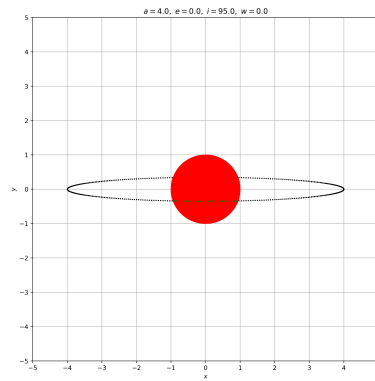
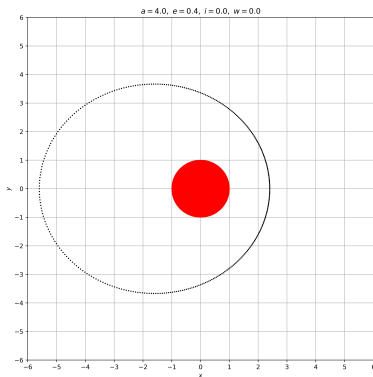
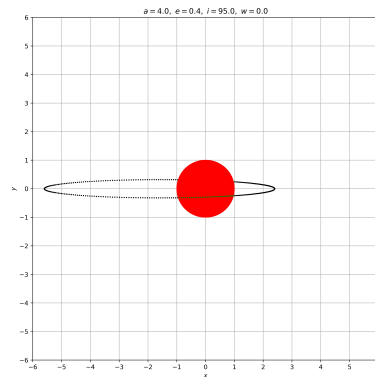
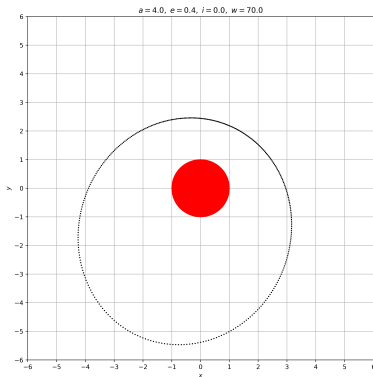
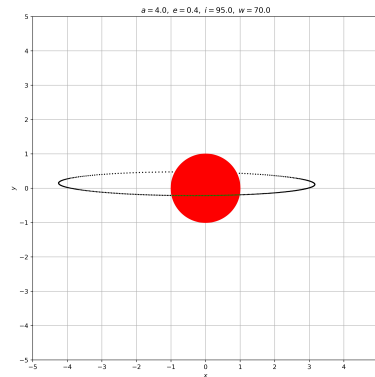
(a)  $e = 0.2$  and  $t_0 = 0.0$ (b)  $e = 0.2$  and  $t_0 = 0.25$ 

Figure 3.2: Elliptical orbit with eccentricity 0.2

### 3.2.2 Orbit Coordinates

(a) Normal view, i.e.  $i = 0^\circ$ (b)  $i = 95^\circ$ Figure 3.3: Setting ( $a = 4.0, e = 0.0, w = 0^\circ$ )(a) Normal view, i.e.  $i = 0^\circ$ (b)  $i = 95^\circ$ Figure 3.4: Setting ( $a = 4.0, e = 0.4, w = 0^\circ$ )(a) Normal view, i.e.  $i = 0^\circ$ (b)  $i = 95^\circ$ Figure 3.5: Setting ( $a = 4.0, e = 0.4, w = 70^\circ$ )

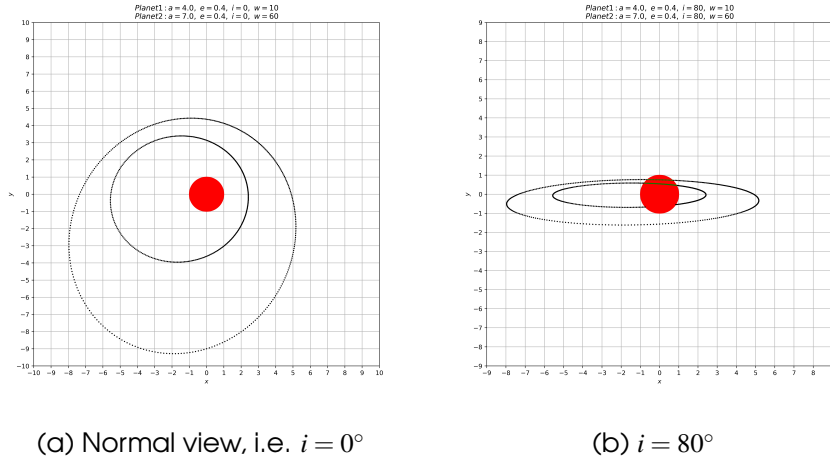


Figure 3.6: Setting ( $a_1 = 4.0$ ,  $e_1 = 0.4$ ,  $w_1 = 10^\circ$ ) and ( $a_2 = 7.0$ ,  $e_2 = 0.4$ ,  $w_2 = 60^\circ$ )

### 3.2.3 Imaging Method

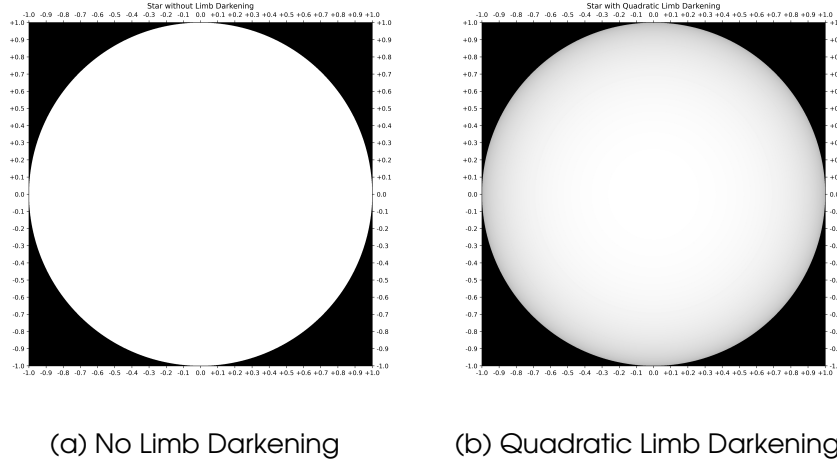


Figure 3.7: Initializing the star with  $1000 \times 1000$  array

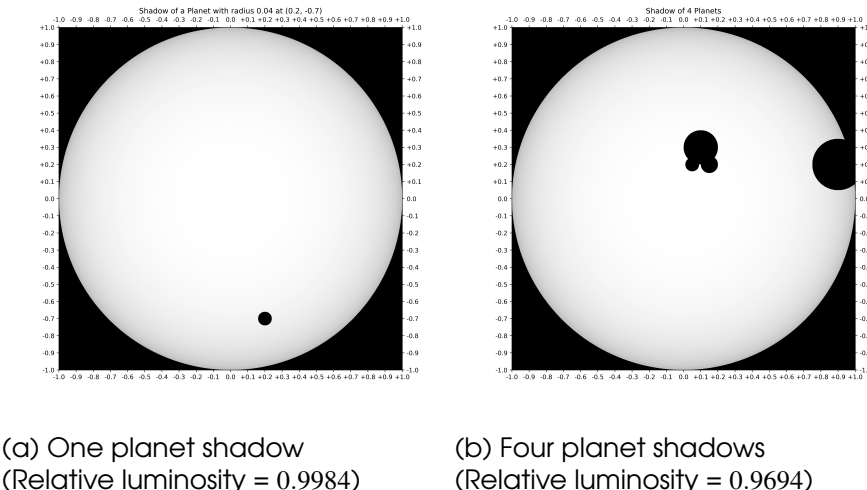
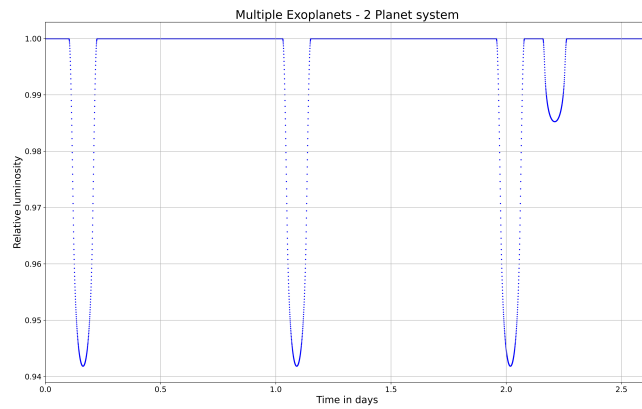
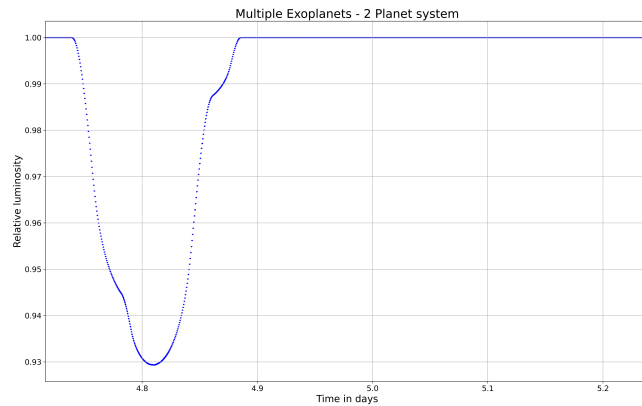


Figure 3.8: Calculating luminosity w.r.t to 3.7b

### 3.2.4 Transit Light Curve for Multiple Exoplanets system



(a) First 3 days with no overlapping transit



(b) Overlapping transit happening on 5th day

Figure 3.9: Simple Two Exoplanet System

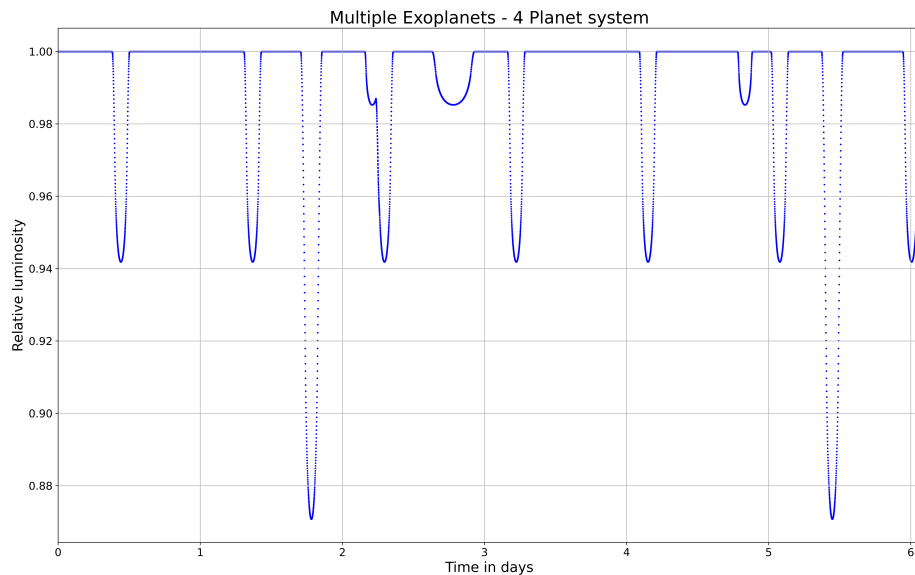


Figure 3.10: Four Exoplanet System

### 3.3 Case Study : TRAPPIST-1 System

TRAPPIST-1 is a brown is an ultra-cool red dwarf star with a radius slightly larger than the planet Jupiter, while having 84 times Jupiter's mass. It is located 39.6 light-years from the Sun in the constellation Aquarius. Seven temperate terrestrial planets have been detected orbiting the star. ([wikipedia.org](https://en.wikipedia.org), 2016)

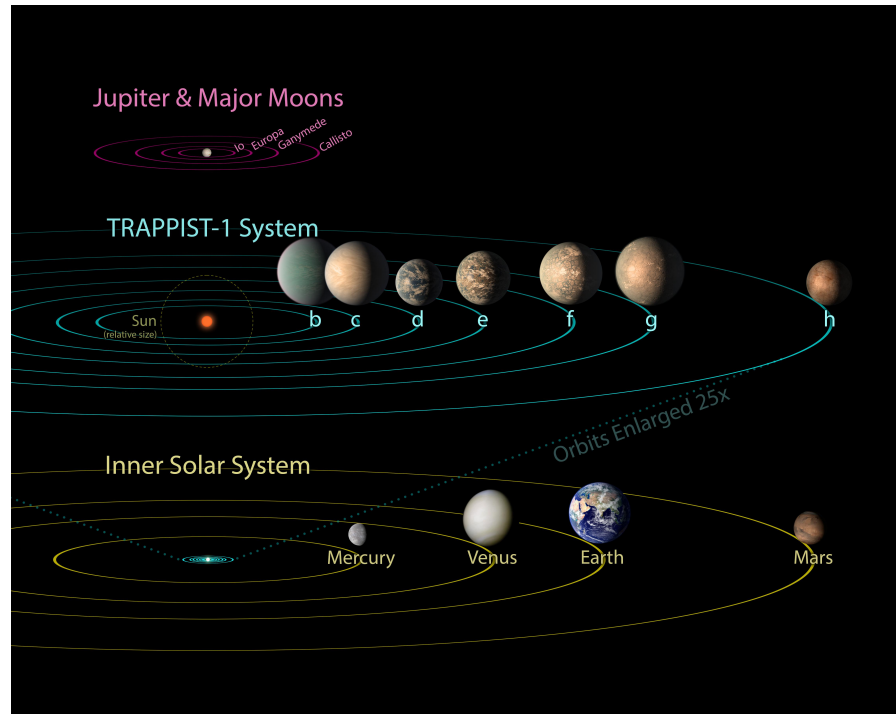


Figure 3.11: Comparing the Trappist-1 system with Solar System and Jovian Moons ([nasa.gov](https://nasa.gov), 2016)

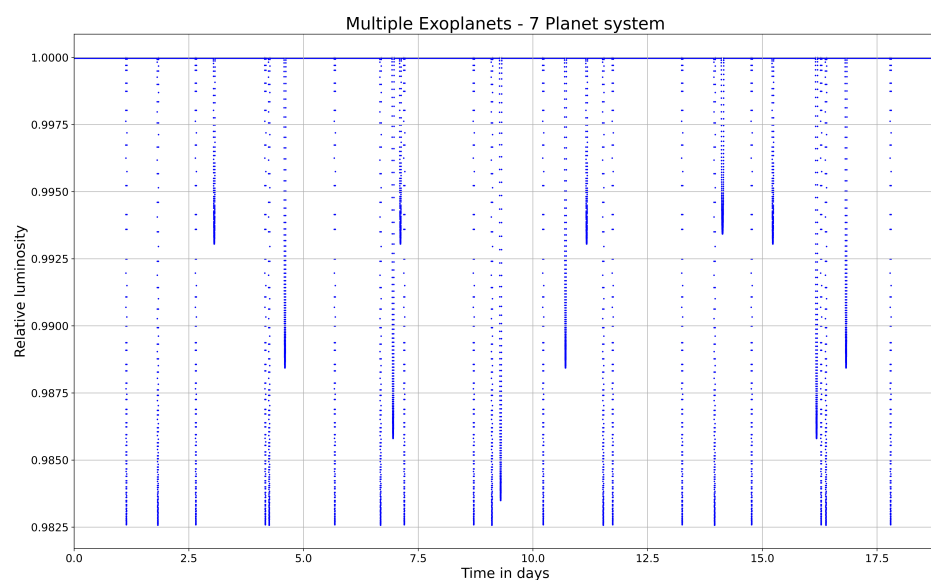


Figure 3.12: Estimated Transit Light Curve using the above mentioned algorithm

### 3.4 Inferences

On observing the Transit Light Curve of Multiple Exoplanet Systems, we can conclude a lot of things about the system - its past, present and future

- **Formation of the system**

The stability of the system can be easily explained by considering the migration of planets to their planets through a protoplanetary disk.

*This is observed in Trappist-1 system.*

- **Age of the system**

If the range of inclination of orbits is large, it can be inferred that the system is young and the planets are yet to settle in proper orbits. Planets migrate to minimize the angular momentum.

*Age of Trappist-1 is somewhere between 5.4 and 9.8 billion years old*

- **The size of orbit**

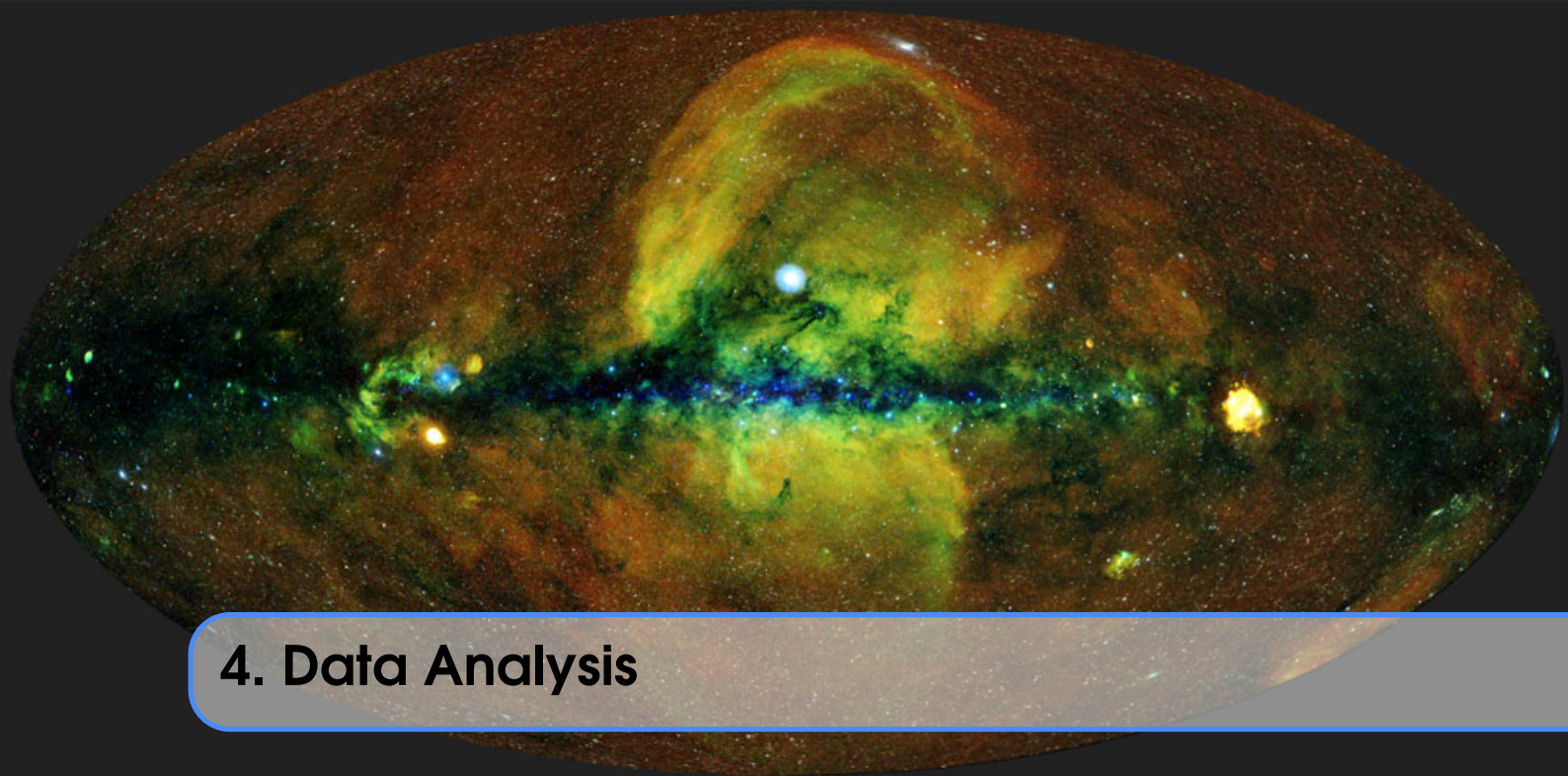
If the orbit size is large, then the transit frequency would be low, thus making it difficult to conclude that an exoplanets orbits the star.

*Orbits of Trappist-1 planets are smaller than Mercury's orbit. Refer Fig. 3.11*

- **The size of star**

As the orbit size is small, the star must not be huge or else it would engulf the planet. So, systems in which we can detect planets would usually have a smaller star.

*Trappist-1 is a red dwarf star*



## 4. Data Analysis

### 4.1 Introduction

Though we have arrived at a pretty accurate model that generates a light curve using analytical methods, this kind of model is not very well suited for us to perform data analysis. A more suitable model would be one that generated the light curve solely through pre-determined formulae as such a model would require far less computational power and run time if we were in a situation where we had to generate multiple models repeatedly. Basically, we condense the model into a single function that generates an array of normalised flux values when the parameters of the exoplanet system are given to the function as arguments.

The formulae used to create such a function are as follows:  
The normalised transit depth  $\delta$ , assuming a dark planet and without considering limb darkening, is given by

$$\delta = \left( \frac{R_p}{R_*} \right)^2 \quad (4.1)$$

where  $R_p$  and  $R_*$  are the radii of the planet and star respectively. The total transit duration for circular orbits with respect to the period ( $t_{T0}$ ), under the assumption that  $a \gg R_*$  and  $\cos i \ll 1$  ( $a$  is the semi-major axis of the orbit and  $i$  is the inclination of the orbit with respect to the plane of the sky), can be derived to be

$$t_{T0} = \frac{R_*}{\pi a} \sqrt{(1 - \delta)^2 - (a \cos i / R_*)^2} \quad (4.2)$$

The total transit duration for eccentric orbits with respect to the period ( $t_T$ ) can be approximated to within a factor of the same quantity for circular orbits. With this, we have

$$t_T \sim t_{T0} \frac{\sqrt{(1 - b)^2(1 - e)^2}}{1 + e \sin \omega} \quad (4.3)$$

where  $e$  is the eccentricity of the orbit,  $\omega$  is the argument of periapsis and  $b$  is the impact parameter given by

$$b = \frac{a}{R_*} \cos i \quad (4.4)$$

Further, if we assume  $t_T \pi \ll 1$ , we get the following relation

$$\left(\frac{t_f}{t_T}\right)^2 = \frac{(1 - \delta)^2 - (a \cos i / R_*)^2}{(1 + \delta)^2 - (a \cos i / R_*)^2} \quad (4.5)$$

where  $t_f$  is the duration of transit without the ingress and egress relative to the orbital period.

Armed with these equations, it is now possible to generate a basic light curve. Limb darkening can be incorporated into this light curve as a factor multiplied to  $\delta$  at each point during the transit. The factor itself can be calculated using the linear limb darkening law, where the "limb darkening angle" is assumed to have a linear correlation with the 2-D distance to the centre of the star. Condensing all of the above into an "all-in-one" function that generates a reasonably accurate light curve, we are now equipped to take on further computationally intensive tasks like data analysis.

In this chapter, we will try to infer the parameters of an exoplanet system and see what set of parameters result in a light curve that best fits a given data set. For this part of the project, we make use of Bayesian Statistics and Markov Chain Monte Carlo (MCMC) methods (especially the Metropolis-Hastings Algorithm) to sample the parameters from a probability distribution and arrive at the best set of parameters.

## 4.2 Bayesian Statistics

Considering probabilities, there are two approaches to solve statistical problems where data is available, and parameters need to be decided for models, so that the data observed can be justified.

1. Frequentist approach - The model parameters are fixed and yet unknown and the data has random fluctuations. Given the model, we try to vary the parameters and models, and select the one which explains the data well. In mathematical notation, this implies a (very) general model of the form  $f(y|\theta)$ . Here, the model  $f$  accepts data values  $y$  as an argument, conditional on particular values of  $\theta$ . Thus, dependent on parameters  $\theta$ , we run the model and see if the results are close to the observed data. For new data, the process needs to be repeated.
2. Bayesian approach - Here, the data is considered absolute, and the model parameters are considered to have a probability distribution. Thus, This implies the form  $p(\theta|y)$ . This formulation used to be referred to as inverse probability, because it infers from observations to parameters, or from effects to causes. Thus, dependent on the data, we find the probability that this data can come from which model and what parameters. For this, we use Bayes' formula.

#### 4.2.1 Bayes' formula

Given two events A and B, the conditional probability of A given that B is true is given by (here  $P(B) > 0$ ) -

$$Pr(A|B) = \frac{Pr(B|A)Pr(A)}{Pr(B)} \quad (4.6)$$

In the above equation, A represents the proposition/model/parameter value and B represents the data.  $P(A)$  is the prior probability of A which expresses its probability distribution or one's beliefs about A before any evidence was known.

$P(B|A)$  is the likelihood, which can be interpreted as the probability of the evidence B given that A is true. The likelihood shows the extent to which the evidence B supports the proposition A.

$P(A|B)$  is the posterior probability, the probability of the proposition A after taking the evidence B into account.

$P(B)$  is called the marginal likelihood, which can be proved to be the sum of the conditional probability of B under all possible events  $A_i$  in the sample space. For example, if we consider two events -

$$P(B) = P(B|A)P(A) + P(B|\bar{A})P(\bar{A}) \quad (4.7)$$

We sometimes ignore this term, as it just serves as a scaling factor, and thus, isn't relevant when finding the maximum value of the posterior probability. The scaling factor serves to limit the posterior probability in the range  $[0, 1]$ , as the axioms of probability theory require.

#### 4.2.2 Why the Bayesian approach preferred?

There is just one estimator in Bayesian inference, which leads to its simplicity. Also we can conceptually use multiple parameters in a simple way; the use of probabilistic models allows very complex models to be easily modelled. Any new parameter can be added easily

Bayesian statistics have coherence. All unknown quantities for a particular problem are treated as random variables, to be estimated in the same way. Existing knowledge is given precise mathematical expression.

Finally, Bayesian statistics confers an advantage in the interpretability of the outputs. Because models are expressed probabilistically, results can be interpreted probabilistically.

#### 4.3 Markov Chain Monte Carlo

A Markov chain is a special type of stochastic process. The standard definition of a stochastic process is an ordered collection of random variables:

$$\{X_t : t \in T\}$$

where  $t$  is frequently (but not necessarily) a time index. If we think of  $X_t$  as a state  $X$  at time  $t$ , and invoke the following dependence condition on each state:

$$\begin{aligned} & Pr(X_{t+1} = x_{t+1} | X_t = x_t, X_{t-1} = x_{t-1}, \dots, X_0 = x_0) \\ &= Pr(X_{t+1} = x_{t+1} | X_t = x_t) \end{aligned}$$

then the stochastic process is known as a Markov chain. This conditioning specifies that the future depends on the current state, but not past states. Thus, the Markov chain wanders about the state space, remembering only where it has just been in the last time step.

The approach of drawing repeated random samples in order to obtain a desired numerical result is generally known as Monte Carlo simulation. If we use Monte Carlo simulation to generate a Markov chain, it is called Markov chain Monte Carlo, or MCMC.

#### 4.3.1 The Metropolis-Hastings Algorithm

There are various algorithms that produce Markov Chains. We will now look at one such algorithm—the Metropolis-Hastings algorithm. In statistical physics, the Metropolis-Hastings algorithm is an MCMC method for obtaining random samples from a probability distribution from which direct sampling is difficult. Though there are better methods for sampling from one-dimensional distributions, this algorithm is quite effective when used for multi-dimensional distributions, especially when the number of dimensions is quite high. As our problem has a dimensionality of 3 (3 parameters to be deduced), we will be using the Metropolis-Hastings algorithm.

The algorithm can draw samples from any target distribution  $P(x)$ , provided we know a distribution  $g(x)$ , which is proportional to the target distribution and easier to work with. The sequence of steps is described as follows:

1. Select initial value  $x_0$ .
2. For  $i = 1, \dots, m$ , where  $m$  is some large number, repeat:
  - (a) Draw a candidate  $x^*$  from a proposal distribution  $q(x^*|x_{i-1})$
  - (b) Compute
 
$$\alpha = \frac{g(x^*)q(x_{i-1}|x^*)}{g(x_{i-1})q(x^*|x_{i-1})}$$
  - (c) If  $\alpha \geq 1$  accept  $x^*$  and set  $x_i \leftarrow x^*$   
 If  $0 < \alpha < 1$  accept  $x^*$  and set  $x_i \leftarrow x^*$  with probability  $\alpha$ .  
 Else reject  $x^*$  and set  $x_i \leftarrow x_{i-1}$  with probability  $1 - \alpha$ .

If the proposal distribution  $q(x^*|x_{i-1})$  is a normal distribution centered about  $x_{i-1}$  as the mean, the algorithm is called “Random walk Metropolis-Hastings” and in this case, the  $q$  terms in the definition of  $\alpha$  turn out to be equal leaving us with

$$\alpha = \frac{g(x^*)}{g(x_{i-1})}$$

Steps (b) and (c) act as corrections as the proposal distribution is not equal to the target distribution. At each step in the chain we draw a candidate and decide whether to “move” the chain there or remain where we are. Since the decision

to move to the candidate only depends on where the chain currently is, it is a Markov Chain.

Our implementation of the Metropolis-Hastings algorithm will be the random walk version.

#### 4.4 Implementation

Firstly a model function that returned an array of normalized flux values, observed during the transit of an exoplanet executing a circular orbit ( $e \sim 0$ ), was created to simplify the process of calculating the posterior of a set of parameters. The model function takes in the radius of the exoplanet, inclination of the orbit and semi-major axis of the orbit as arguments and returns the desired array of values, using the pre-specified value of the radius of the host star (the period is not significant as the values taken are against normalised time). A light curve was obtained with the help of the above model function, using the parameters of a typical exoplanet system and Gaussian noise was injected into this to simulate real data.

The posterior distribution function (probability density function) was then defined as follows:

Let  $d_i$  be a data point and  $m_i$  be the corresponding point in the model. We have

$$r_i = (d_i - m_i)^2$$

where  $r_i$  is the corresponding ‘residual’. Let  $s$  be the sum of residuals defined as

$$s = \sum r_i$$

We then define the likelihood  $l$  as

$$l = e^{\frac{-s}{2\sigma^2}}$$

where  $\sigma$  is the standard deviation of the detector noise, which we know. Assuming uniform priors, we have the un-normalised posterior ( $p$ ) to be

$$p = l$$

where we have assumed the prior to be 1.

A function that implemented the MCMC algorithm and returned an array of accepted sample values by drawing samples from a pre-specified range of priors, was created and the chain was run with the necessary input parameters.

#### 4.5 Plots

In Fig 4.1, we can see that parameter ‘burn-in’ is occurring quite well for the radius of planet and semi-major axis parameters while the chain is still wandering a bit for the inclination parameter. Nevertheless pre-burn-in samples were discarded and the chain was further thinned by accepting samples that had lesser correlation (i.e independent samples).

A histogram was plotted (Fig. 4.2) for the new set of accepted samples and compared with the injected parameter values (the system parameters that were used to create the data).

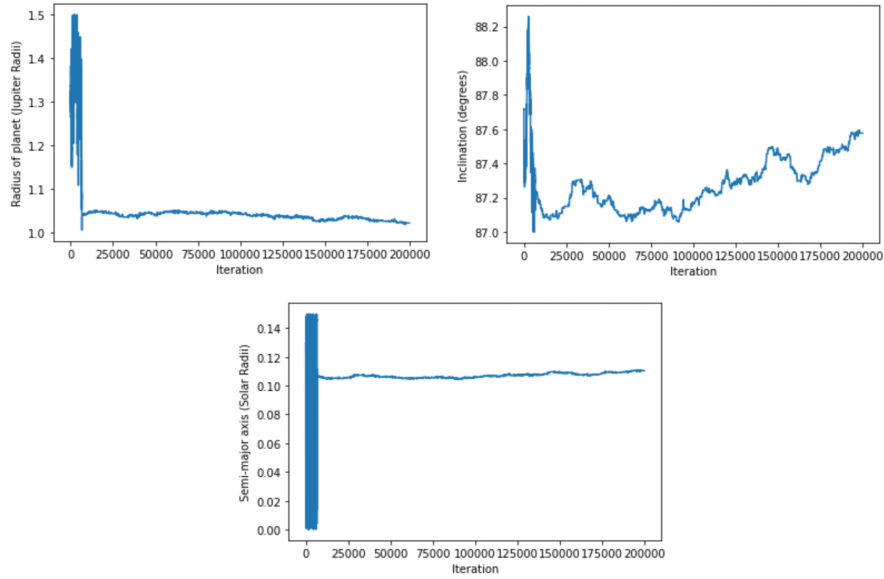


Figure 4.1: Samples taken by chain vs iteration.

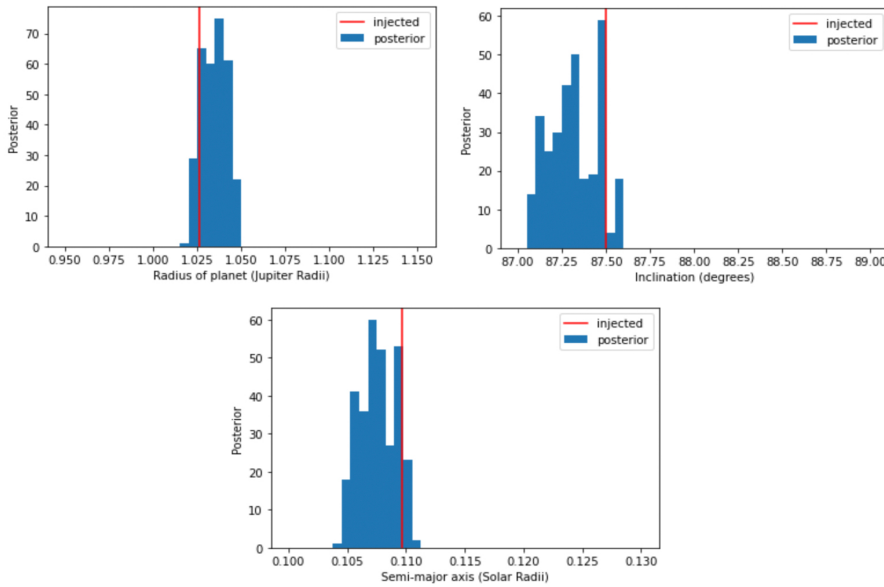


Figure 4.2: Histogram of the parameters taken up by chain

## 4.6 Inference

As can be seen in Figure 4.1, parameter burn-in is not occurring so well for the inclination parameter ( $i$ ). We see that it does not require significant change in the radius of planet ( $r_p$ ) and semi-major axis ( $a$ ) parameters to balance out the change in  $i$  and give a reasonably ‘good fit’ to our data. The ‘wandering’ of the chain for the  $i$  parameter just tells us that it is a very sensitive parameter compared to the other two.

In spite of this, the histogram tells us that the chain has settled down onto parameter values that are not that far away from the injected values. Superimposing

our data with the light curve generated by the model function, using the ‘most likely’ set of parameters obtained from our MCMC algorithm, we get Fig 4.3.

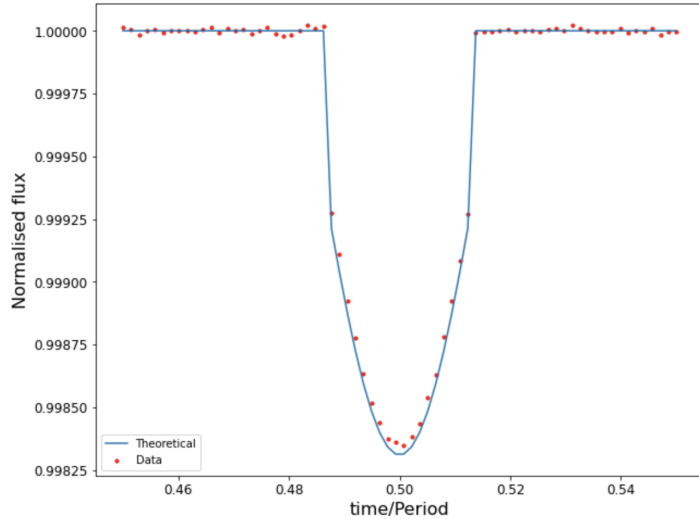


Figure 4.3: The data superimposed over the light curve obtained from the model, using the parameters predicted by the MCMC algorithm

## 4.7 Challenges

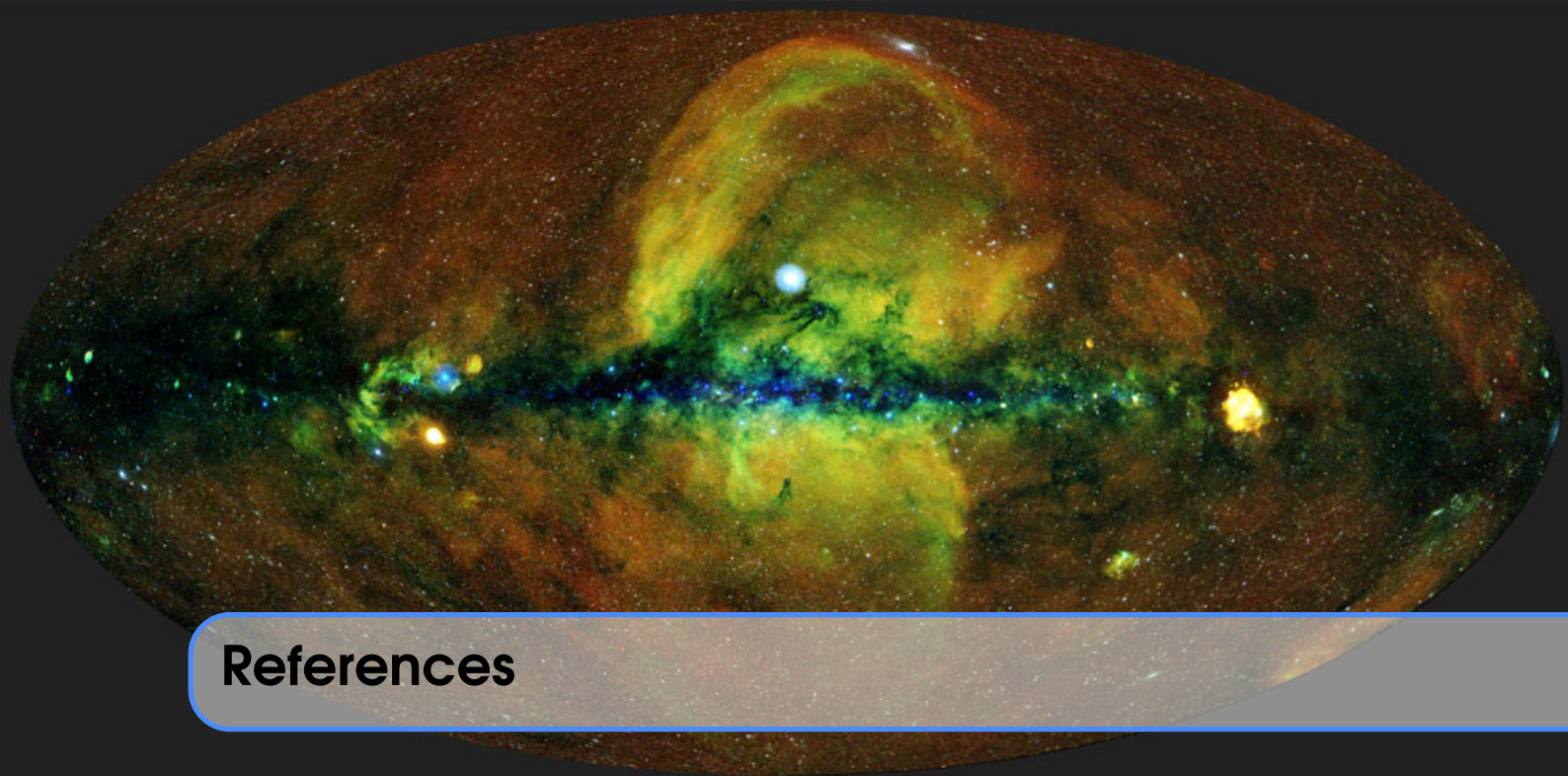
- Since the data and the model function deal with normalised flux values, it is only possible to deduce the ratio of the radius of the planet ( $r_p$ ) to the radius of the star ( $r_s$ ) as the relative dip in the intensity of light observed depends only on this ratio. Hence to determine  $r_p, r_s$  needs to be known.
- Even after specifying a range of priors (from which the MCMC algorithm chooses its samples randomly), it is possible that the chain chooses a set of parameters such that the exoplanet transit may not be observable. Physically, this means that the exoplanet does not block out any portion of the host star throughout its orbit ( $b > 1$ ). But, mathematically this amounts to negative values being encountered in the square roots used to calculate some properties of the exoplanet system, which ultimately results in run-time errors. A work-around to this problem was to include a few lines of code in the MCMC algorithm that accepted samples that satisfied the conditions for transit.
- Usually, a large prior range is specified for sensitive parameters like  $i$  to ensure good burn-in when the chain is run. But, doing so was not practical in our particular case. Though it is possible to accept only those samples that satisfy the condition for transit, it is practical to check this condition only for new samples. As the chain chooses a random starting point, it is quite possible that the parameters chosen do not satisfy the conditions for transit and the probability that a non-transit set of parameters is chosen initially, increases tremendously upon increasing the range of priors. If a large prior range is specified for  $i$ , it would take quite a bit of luck to arrive at a value for the random seed that would result in an initial set of parameters satisfying the

transit condition. Thus, the prior range for  $i$  was kept as  $87^\circ - 90^\circ$  at the cost of incomplete burn-in.

#### 4.8 Discussion

The method that we have used here to fit the data is extremely basic. Ideally, the process of parameter inference requires the running of multiple chains with different starting points. Only if all the chains converged to a similar set of parameters, would we be satisfied with the obtained results. Also, a more realistic data analysis exercise would be to use real data and deduce all the basic parameters, including the period and eccentricity. This would invariably involve a more practical model that generated a light curve (without a fixed starting point) for multiple transits.

Another point to note is that as we are using self-engineered data to understand the process of parameter inference, we know the standard deviation of the noise that we injected to create the data. We make use of this information to calculate the likelihood in the posterior distribution function. However, if we are dealing with real data, we would have to manually deduce the ‘detector noise’ to calculate the posteriors accurately. For doing so we would have to sample the points that are not part of the transit and calculate the standard deviation of these points about 1 (for normalised flux). Only then would we be able to run the MCMC algorithm.



## References

- Alapini Odunlade, A. E. P 2010
- Claret, A. 2000, Astronomy and Astrophysics, 363, 1081
- Elíasdóttir, Á., Hjorth, J., Toff, S., Burud, I., & Paraficz, D. 2006, The Astrophysical Journal Supplement Series, 166, 443
- <http://exoplanet.eu/>. 2020, <http://exoplanet.eu/catalog/>
- Kramer, M. 2018, haex, 5
- Lovis, C., & Fischer, D. 2010, Exoplanets, 27
- Mayor, M., & Queloz, D. 1995, Nature, 378, 355
- Meneghetti, M. 2006, Lecture Notes organized in a course on web, <http://www.ita.uni-heidelberg.de/~massimo/sub/glensing.html>
- microlensing source.org. 2017, <https://microlensing-source.org/concept/point-lenses/>
- Moon, B., Jeong, D.-G., Oh, S., & Sohn, J. 2017, Journal of Astronomy and Space Sciences, 34, 99
- Morello, G. 2016, PhD thesis, UCL (University College London)
- nasa.gov. 2016, <https://photojournal.jpl.nasa.gov/jpeg/PIA22096.jpg>
- Ramesh Narayan, M. B. 1997, Lecture notes in arXiv.com, 53
- Schneider, J. 2002, arXiv preprint astro-ph/0210622
- Sing, D. K. 2010, Astronomy & Astrophysics, 510, A21

- Triaud, A. H. 2017, arXiv preprint arXiv:1709.06376
- wikipedia.org. 2016, <https://en.wikipedia.org/wiki/TRAPPIST-1>
- Wolszczan, A., & Frail, D. A. 1992, *Nature*, 355, 145